The Second Symposium on Theories and Applications of Basic and Biosciences

Organized by the Bioresearch and Consultancies Office- Misurata University with the Collaboration of the Faculty of Science

Previewed Scientific Symposium

5/9/2015

The Second Symposium on Theories and Applications of Basic and Biosciences

Vol. 2 Issue 1 5 September 2015

Correspondences:

Journal of Science,

Faculty of Science,

Misurata University,

PO Box 2478,

Misurata, Libya.

Email:

journalofscience2013@gmail.com

Contents

The Effects of Genetic, Epigenetic and Environmental Factors on Dental Development: A Phenotypic Analysis of Monozygotic Twins

A.M. Hmeida[1], A.O.Elraaid[2], M.A. Ablal[3], G.C. Townsend [4]

[1,2]Dental Sciences Department, College of Medical Technology, Misurata, Libya
[3]School of Dentistry, The University of Liverpool, Daulby Street, Liverpool L69 3GN, UK
4- School of Dentistry, University of Adelaide, SA 5005, Australia

Abstract—The influence of genetic, epigenetic and environmental factors in dental development can be understood by the study of tooth of twins. This study aims to investigate the dental fluctuating asymmetry of tooth dimensions in monozygotic (MZ) co-twins as a measure of how dental development is affected by epigenetic and environmental factors.
Keywords: Twin studies, genetic, epigenetic, environmental, dental development, asymmetry

INTRODUCTION

Twin studies provide a useful approach to investigate the roles of genetic and environmental factors in tooth development.[1] Heritability of different dental traits can be determined from such studies .[2] From the genotypic contribution to phenotypic variation ,heritability can be quantified and presented into two types: 'broad sense' and 'narrow sense'. By comparing the similarities between monozygotic (MZ) twin pairs with those between dizygotic (DZ) twin pairs, estimates of heritability can be determined. Studies involving MZ co-twins have proved to be a powerful tool for investigating the roles of genetic and epigenetic factors which affects cells without affecting its DNA and environmental factors or external conditions and their interaction in determining quantitative traits such as tooth size and form.[3]
Variation in dental crown size can be measured on contra lateral sides of the dental arch, Therefore, the study of asymmetry is a means of investigating stability of a developmental process and providing a measure of developmental interference with the "genetic blueprint" during ontogeny.[5]
Aims:
The aim of this study was to assess the reliability and validation of a 2D dental image analysis system on the measurement of MZ dental cast samples. An attempt has been made to quantify the dental asymmetry as a measure of epigenetic and environmental factors affecting dimensions of permanent teeth of MZ co-twins .

MATERIALS AND METHODS

The 2D image analysis techniques using a Kodak DCS Pro SLR digital camera (Figures 1 and 2) of measurement were used to record the mesiodistal (M-D), buccolingual (B-L), the area (A), and perimeter (P) of permanent teeth of MZ co-twins[6]. Twenty sets of dental study models of MZ twins from Adelaide, South Australia were selected for measurement. Duplicate models were stored in the University of Liverpool. Internal university ethical approval was granted (RETH000063). The tooth types measured on each model were the

central incisor, lateral incisor, second premolar and first molar in each of the four quadrants.

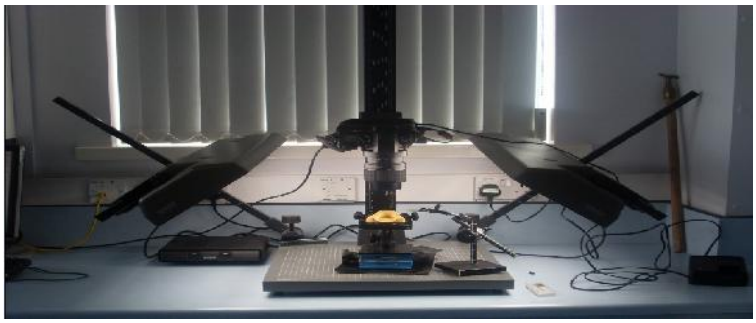

Figure 1 : The camera, computer, the stand and the source of illumination used in this study

Figure 2 : Kaiser copy stand and the model stand with the dental cast.

Bland and Altman plots[7] were used as a pictorial representation to observe the limits of agreement and spread of data for inter-operator reproducibility. Bias calculations were then performed to assess the significance of any bias observed.

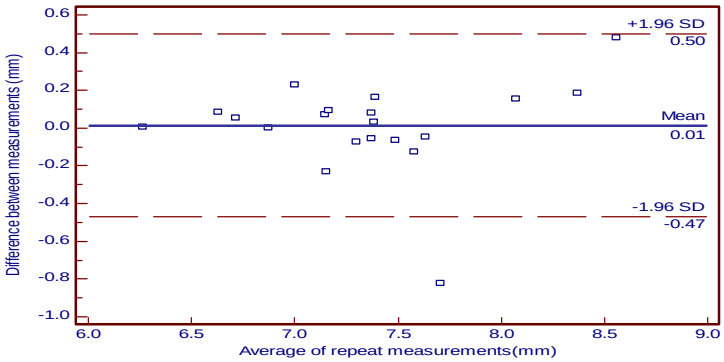

Figure 3: Bland and Altman Plot for Intra-operator repeatability for UR1 BL (occlusal view).Mean Dif. (0.01) < 0.11 (1.96 X SE) and therefore implies no significant bias.

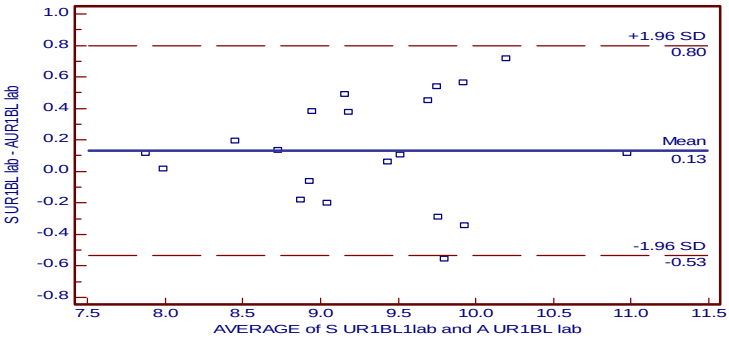

Figure 4: Bland and Altman Plot for Inter-operator repeatability or UR1 BL (occlusal view).
Mean Dif. (0.13) <0.15 (1.96 X SE) and therefore implies no significant bias.

RESULTS

Table 1: 2D Intra-operator repeatability descriptive statistics for the upper right central (labial and occlusal views) and second premolar (occlusal view) teeth.

Variable	UR1 Labial				UR1 Occlusal				UR5 Occlusal			
	MD	OG	A	P	MD	BL	A	P	MD	BL	A	P
ICCC	0.71	0.82	0.97	0.71	0.73	0.90	0.91	0.93	0.86	0.93	0.92	0.90

Table 2: 2D Intra- operator repeatability descriptive statistics for the upper left lateral (occlusal view) and upper left first molar (occlusal view) teeth.

Variable	UL2 Occlusal				UL6 Occlusal			
	MD	BL	A	P	MD	BL	A	P
ICCC	0.96	0.64	0.98	0.79	0.98	0.98	0.97	0.66

Table 3: 2D Inter-Operator reproducibility descriptive statistics for the upper right central (labial and occlusal views) and second premolar (occlusal view) teeth.

Variable	UR1 Labial				UR1 Occlusal				UR5 Occlusal			
	MD	OG	A	P	MD	BL	A	P	MD	BL	A	P
ICCC	0.64	0.89	0.88	0.79	0.83	0.73	0.81	0.74	0.76	0.81	0.81	0.77

Table 4: 2D Inter- operator reproducibility descriptive statistics for the upper left lateral (occlusal view) and upper left first molar (occlusal view) teeth

Variable	UL2 Occlusal				UL6 Occlusal			
	MD	BL	A	P	MD	BL	A	P
ICCC	0.90	0.64	0.74	0.63	0.84	0.51	0.84	0.59

CONCLUSIONS

2D image analysis facilitated the additional measurements of surface area and perimeter. Asymmetry between twin pairs for each tooth type followed a pattern fitting with the morphogenetic field theory with the key teeth showing the least asymmetry (higher centrals, higher sixes, lower laterals, lower sixes) and the variable teeth showing the most asymmetry (higher laterals , higher fives and lower sixes).

The results suggest that whilst gene interaction is significant in the predisposition of dental development in relation to fields of tooth type, environmental pressures are also responsible for any differences

REFERENCES

[1] Townsend G.C., Hughes T., Lucianio M., Bockmann M. and Brook A. (2008) Genetic and environmental influences on human dental variation: a critical evaluation involving twin studies. Arch of Oral Biol. (In press)

[2] Dempsey PJ and Townsend GC. Genetic and environmental contributions to variation in human tooth size. Heredity 2001;86:685-693.

[3] Martin N.G., Boomsa D and Machin G. (1997) A twin prolonged attack on complex traits. Nat Genet 17: 387-392.

[4] Pangrazio-Kulbersh V and Berger JL. (1993) Treatment of identical twins with Frankel and Herbst appliances: a comparison of results. Am J Orthod Dentofacial Orthop. 103:131-137.

[5] Klingenberg CP., Barluenga M and Meyer A. (2002) Shape analysis of symmetrical structures: quantifying variation among individuals and asymmetry. Evolution.56:1909—20.

[6] Brook A.H., Smith R.N., Elcock C., Al-Sharood M.,Shah A and Karmo M. (1999)The measurement of tooth morphology: development and validation of a new image analysis technique. A.Brook (ed. Current trends in dental morphology research), Sheffield Academic Press: 380-387.

[7] Bland.J.M and Altman.D.G. (1986) Statistical methods for assessing agreement between two methods of clinical measurement. Lancet. 6:147-157.

The Second Symposium on Theories and Applications of Basic and Biosciences5 September 2015

White Variant of *Trichophyton Violaceum* Isolated in Misurata, Libya

Alfaitouri, K.O

Department of laboratory, Technology college, Misurata , Libya .
E-mail: alfaitouriko@yahoo.com

Abstract— Dermatophytes are geographically restricted and endemic in particular parts of the world, while other species may have a sporadic but worldwide distribution. *Trichophyton violaceum* is one of the most common dermatophytes causing tinea capitis, and is the predominant cause of tinea in Africa,. Among 22 dermatophyte transmission from human to human (Anthropophilic fungus *T.violaceum)* isolates collected from school children with tinea capitis, isolate had uncharacteristic phenotypic features. Based on conventional methods in mycological center of Assiut university, this isolate was identified as white variant of T. violaceum. This is the first time that white isolate of *T. violaceum* have been identified in Misurata

Keywords- dermatophytes, Anthropophilic fungus, tinea capitis, phenotypic, Trichophyton violaceum, Africa, Misurata

INTRODUCTION

Cutaneous fungal infections can be caused by dermatophytes, yeasts although dermatophytes cause most of the cutaneous fungal infections, The dermatophytes are a group of closely related fungi that have the capacity to invade the keratinized tissue (skin, hair and nails) of humans and other animals to produce an infection, dermatophytosis, commonly referred to as ringworm or Tinea , is an infection caused by dermatophyte fungi belonging to the genera Trichophyton, Microsporum and Epidermophyton.1 Tinea capitis is a dermatophyte infection of scalp and hair [1] [2] [3] [4] . Infections are generally restricted to the skin and they do not penetrate the deeper tissue or organs of immunocompetent hosts [5]. *Trichophyton violaceum* is one of the most common dermatophytes causing tinea capitis [6] . There are two main patterns of tinea capitis infection: ectothrix and endothrix infections. In ectothrix infections, fungal arthroconidia cover the outside of infected hairs, which eventually break off a few millimeters above the scalp surface, for example those caused by the an thropophilic species (eg. *Microsporum audouinii*) to or zoophilic (eg, *Microsporum canis*) or soil-associated geophilic (eg. *Microsporum gypseum*) dermatophytes. In endothrix infections, for example those caused by the anthropophilic species Trichophyton tonsurans, *Trichophyton violaceum* or, the fungus is confined to the interior of the hair shaft. Infected hairs become very fragile, breaking off level with the follicular orifice and producing black dot [7] [8].

MARTIAL AND METHODS

A total of 22 patient samples (schoolchildren) , ages7-15 years, including, hair roots and skin scrapings., analyzed by direct microscopy and culture. Microscopic examination of these specimens was carried out in KOH (10%) and cultured on SDA with, thymine and chloramphenicol, cycloheximide and Dermatophyte Test Medium (DTM) . Cultures were

incubated at 25°C for up to 28 days and checked twice weekly for growth. Identification of dermatophyte isolates was on the basis of microscopic morphology [2] [3] [6] .

RESULT AND DISCUSSION

KOH examination of hair showed endothrix parasitism [Fig.1] Reddish purple colonies were isolated from the patient on Sabouraud's dextrose agar, and intercalary chlamydospores were observed. Secondary cultures in Dermatophyte Test Medium (DTM) turned the medium red, indicating the possible presence of a dermatophyte.
Therefore, the isolated fungus was identified as T. violaceum, but one isolate had uncharacteristic phenotypic features. this isolate were identified as white variant of T. violaceum. This is the first time that white isolates of T.violaceum have been identified in Misurata[Fig.2] Based on conventional methods in mycological center of Assiut university The result is similar to that of Woldeamanuel et al [9]. Tinea capitis is mainly a disease of infants and children and its prevalence of closely related to socioeconomic status and life style and commonly occur under poor hygienic conditions [10] . In the present study children of 7-9 years old were the most affected group with 77.27% compared to 22.73 % in children of 10-12 years old [11][12] . females were less affected showing 40.91 % to 59.09 % for male [13] [14] [15] . *T. violaceum* was the most common cause of tinea capitis [11] [13] [16][17] [18] [19] . Living conditions, large family size and close contact, either directly or by sharing facilities, including combs and towels [10] .

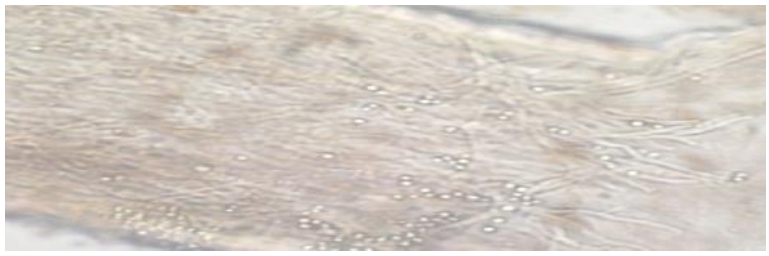

Fig. 1 Positive KOH examination of hair (Endothrix).

Fig. 2 White variant of *T. violaceum* white in SDA

CONCLUSION

This case represent the first time of infections caused by the white variant of *T. violaceum* in Misurata, Libya . The case reported here in raise assigning special importance

to its accurate identification in the laboratory.

ACKNOWLEDGEMENTS

I acknowledge Dr. Ahmed Mlitan , Dr.Taher Alhabge and also acknowledge mycological center of Assiut university, Eygpt . and. I would also like to thank the staff and children at the school.

REFERENCES

[1] B .A. Forbes, D.F. Sahm& A.S. Weissfeld"Bailey &Scott's diagnositic microbiology ," diagnositic microbiology ed 12th, Mosby Elsever Missouri , 2007,chapter 50, Pp 629- 635

[2] K.J. Kwon-Chung& J.E. Bennett"Medical mycology ," Lea & Febiger USA , 1992 ,chapter 6 Pp105-161

[3] D.H. Larone "Medical impotant fungi: aguide to identification," ed 3rd , 1995 ,Pp (161-181 ,216-217)..

[4] I.Weitzman & R.C. Summerbell " The dermatophytes," Clin Microbiol Rev 1995;8:240-59. [PUBMED]

[5] P.G. Sohnle " Dermatophytosis, fungal infection and immune response In Immunology of the fungal diseases ," In: Cox RA, editor. Boca Raton FL: CRC press; 1989. p. 27-47..

[6] D.Frey, R.J. Oldfield & R.C. Bridger,"AColour Atlas of Pathogenic Fungi ,"General Editor Wolfe Medical Publication Ltd Holland , 1979, Pp 68-69

[7] R.J .Hay& M.K. Moore, "Mycology. In: Burns T, Breathnach S, Cox N, Griffins C, eds. Rook's textbook of dermatology," Vol 2. 7th ed. Oxford: Blackwell Science, 2004: 1405-1506

[8] A.K. Gupta & R.C. Summerbell ," Tinea capitis ," Med Mycol, 2000; 38: 255-287.

[9] Y.Woldeamanuel , R Leekassa,. B. Petrini & U. Chryssanthou "White variants of *Trichophyton violaceum* isolated in Ethiopia ," APMIS. 2005, ; 113(10):708-12

[10] S .B. Jahromi & A.A. Khaksar , "Aetiological agents of tinea capitis in Tehran (Iran) ," Mycoses, 2006;49:65-7.

[11] A.M. Gargoom, M.B . Elyazachi , S.M. Al -Ani & G.A. Duweb , "Tinea capitis in Benghazi, Libya ," , Int. J. Dermatol , 2000; 39(4):263-5

[12] A.A.Omar,"Ringworm of the scalp in primary-school children in Alexandria: infection and carriage ," East Mediterr Health. J. 2000 ; 6(5-6):961-7.

[13] A.M. Nawaf, A.Joshi, A. Zaki, O. Nour-Eldin, M. AI- Sheltawy, I .El- Adawy & A.K. Sharma , "Tinea capitis among children and adolescents in the Farwaniya region of Kuwait," J. Dermatol, 2003 ; 30(12):904-909

[14] H.I..Fathi & A.M. Al-Samarai "Tinea capitis in Iraq: laboratory results ," East Mediterr Health J , 2000 ;6(1):138-48

[15] M.S. Ali-Shtayeh & H.M. Arda "Epidemiological study of tinea capitis in schoolchildren in the Nablus area (West Bank) ," Mycoses . 1998;41(5-6):243-8

[16] Y. K. Malhotra, M. P. Garg, A.J . Kanwar & S. Nagrajan, "A study of Tinea capitis in Libya (Benghazi) ," Sabouraudia , 1979 ;17(3) :181-3.

[17] T.Othman &C. Vacher ," Tinea of the scalp in Egypt ," Bull. Soc. Pathol. Exot .Filiales, 1983;76(2):126-8.

[18] M.S. Ali-Shtayeh & H.M. Arda, "A study of tinea capitis in Jordan (West Bank).," J .Trop. Med. Hyg , 1986 ; 89(3):137-41.

[19] M.S.Ellabib, M. Agaj , Z . Khalifa, & K. Kavanagh, "*Trichophyton violaceum* is the dominant cause of tinea capitis in children in Tripoli,Libya; result of a two year survey ," Mycopatholgia, 2002 ;153(3) :145-7 .

Analysis of some Heavy Metal in Marine Fish in Muscle, Liver and Gill Tissue in Two Marine Fish Spices from Kapar Coastal Waters, Malaysia

Fathi Alhashmi Bashir[1] and Esmail Mohamed Alhemmali[2]

[1]Animal Production Department, Veterenary and Agriculture Sciences Faculty, Al-zawia University, Al-zawia, Libya.
[2]Zoology Department, Faculty of Science, Misurata University, Misurata, Libya
[2]Corresponding Author's email: f.elhashmi@yahoo.com

Abstract— This study was conducted to ascertain the levels of heavy metals, namely cadmium, copper, lead and zinc in muscle, liver and gill tissues in two marine fishes Pennahia anea and Arius maculatus. The results showed that the concentrations of heavy metals were higher in liver and gill than in muscle. Zn concentration was found highest in all species in different seasons. The seasonal variations of Cu, Zn and Cd in tissues revealed that these metals were higher concentrated during rainy seasons. However, in dry season, Pb concentrations in the muscle were higher than the maximum levels set by FAO/WHO but still below the Malaysian food regulation standard. The results of the current study indicated that heavy metals in the edible parts of the investigated fish are in the permissible safety levels for human consumption.
Keywords– safety level, marine fish, metals.

INTRODUCTION

Pollution has been very damaging to aquatic ecosystems, and may consist of agricultural, urban, and industrial wastes containing contaminants that have proven to be harmful to aquatic habitats and animal species [1]. For these reasons, it is important to determine the chemical quality of the marine organisms, particularly the contents of heavy metals, in order to evaluate the possible risk of fish consumption by humans [2]. Metals such as Cu and Zn are essential metals, since they play an important role in biological systems. Which are required for metabolic activity in organisms, lie in the narrow "window" range between their essentiality and toxicity. Other heavy metals like Pb and Cd, which are non-essential metals, may exhibit extreme toxicity, even in trace concentrations under certain conditions, require necessitating regular monitoring of sensitive aquatic environments [3]. The essential metals can also produce toxic effects when their intake is excessively elevated. Levels of heavy metals in fish have been widely reported [4-6].

Fish becomes the major part of the human diet due to its high content of proteins, low cholesterol and high percentage of omga3 polyunsaturated fatty acids (PUFA) such as eicosapentaenoic acid (EPA) and docosahexaenoic acid (DHA), liposoluble vitamins and essential minerals [7, 8]. Furthermore, in many studies, fishes are the subject of investigations on heavy metal accumulations and monitoring programs in seas, due to their importance in human nutrition [9, 10]. Metal absorption in fish is carried out via two main uptake routes: gills surface (water exposure) and digestive tract (diet exposure) [11]. Gills are one of the most critical organs in terms of metal toxicity in fishes [12], as they are in direct contact with the water and are a site for uptake of metals [13]. In fish, disruption of ion transport across the gills is a major cause of toxicity [12]. After being absorbed by the gills, metals are further transferred via blood to other target organs, such as the liver and

kidney. The liver has a high metal accumulating capacity and is one of the most specialized tissues for metal metabolism, performing important and complex biological functions like energy metabolism that are essential for survival [14]. On the other hand, fish muscle is not an active tissue in accumulating metals with the exception of organic mercury [14].
The most common toxic effects of metals are involve the brain and kidneys. Lead exposure can cause a wide spectrum of health problems, ranging from convulsions, coma and renal failure. Acute high dose of cadmium exposure can cause severe respiratory irritation, while long-term cadmium exposure has proven to be a risk factor for chronic lung disease and testicular degeneration. According to [4], zn is vital for normal metabolism for the schools of fishes. Camara et al. [15] have established the health benefits of advocated level of mineral consumption. They claim that deficiency of Zn will cause loss of appetite, growth retardation, skin changes, and immunological abnormalities. Copper is an essential element and is carefully regulated by physiological mechanisms in most organisms [16]. However, it is regarded as potential hazards that can endanger both animal and human health. Results show that metal concentrations in fish muscles vary widely, depending on the location of capture. Several studies have shown that the accumulation of heavy metals in tissues is primarily dependent upon the needs, sex, size and molt of marine animals and also upon the water concentrations of metals and the exposure period, while other environmental factors such as salinity, pH, hardness and temperature also play significant roles in metal accumulation [4, 17].
Kapar marine ecosystem is stressed ecosystem selected as it is located in the Strait of Malacca which consists of many pollution sources situated around it. This locality gets infected by a great variety of pollutants due to the existence of large number of international shipping lanes and the concentration of agricultural, industrial, and urbanizal activities along the coast of Peninsular Malaysia [18]. Moreover, the Strait of Malacca is one of the most vulnerable areas to contamination by oil spills [19]. On the other hand, the Strait of Malacca is the most important fishing ground in Malaysia, accounting for approximately 70% of total fish landings of the country [19]. Apart from the above-mentioned sources of pollution, an electric power station that uses coal and discharges the polluted, perused water into the surface water systems surrounding Kapar, also contribute to the heavy metal pollution of the marine ecosystem in this area. Moreover, Kapar has great importance for the local fishery industry. Therefore, it is vital to estimate the selected metals in fish of the Kapar coastal water to define the current heavy metal levels in the fish as well as to monitor the trends of change in fish metal levels in relation to time. The objectives of the present study were to determine the concentration of heavy metals (Cu, Zn, Cd and Pb) in muscles, livers and gills of two fish species, P. anea and A. maculatus collected from Kapar Coastal Waters, Malaysia. Moreover, to investigate the seasonal variation of the same heavy metals between the dry and rainy seasons.

MATERIALS AND METHODS

Samples collection:
Twenty specimen of fishes were collected seasonally from Kapar coastal water on the western coastal water of Malaysia (Figure 1) in March and April as dry season, October and November as rainy season 2009. The fish species P. anea and A. maculates were caught from the same site during March, April, October and November.

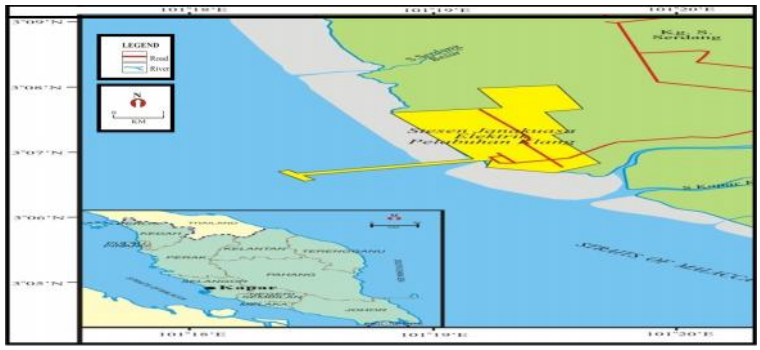

Figure 1. Sampling areas near Coal Power Station of Sultan Salahuddin Abdul Aziz, Kapar, Selangor

These species are commonly consumed by the local population in Malaysia. Specimens collected during the sampling period were immediately transported to the laboratory in ice. Total length and weight of the specimen were measured to the nearest centimeter and gram. Fish guts, muscles, livers and gills were removed with a plastic knife and weighed and homogenized for metal analysis. Individual separated were dried in oven to constant weight at 80 C° in acid-washed petri dishes.

Microwave digestion procedures:
The digestion was performed in a microwave digester with 3 ml of HNO_3 (65% v/v), 1 ml of H_2O_2 (30% v/v) to prepare the samples for analysis, with a microwave oven (Start D Closed Vessel Microwave Digestive System) using the microwave digestion program. All metal concentrations were determined on a dry weight basis as µg/g. A blank digest was carried out in the same way. Detection limits were determined as the concentration corresponding to three times the standard deviation of ten blanks. All metals were determined against aqueous standards. Digested samples were analyzed three times for each metal. In order to validate the method for accuracy and precision, certified reference materials of muscle tissue (SRM 2976, National Research Council, Canada) were analyzed for corresponding elements.

Analytic procedures:
Determination of all metal concentrations of Cu, Zn, Cd and Pb were carried out by inductively coupled plasma mass spectrometry (ICP-MS, Perkin Elmer model Elan 9000, USA). After calibrating the instrument with standard solutions derived from commercial materials, it was optimized according to the manufacturing standards. The quality of data was checked by the analysis of standard reference material of marine biota sample (SRM2976, freeze dried muscle tissue, National Institute of Standards and Technology, USA).

RESULTS

The results showed good agreement between the certified and the analytical values Table (1).Statistical analysis of data was carried out using SPSS statistical package program. Three-way analysis of variance (ANOVA) and Duncan multiple range tests were used to assess whether metal concentrations varied significantly among tissues seasonally. As the distribution of metals data was markedly skewed, logarithmic transformations of the data were applied.

Table 1. Recovery of metals in muscle tissue certified reference materials (SRM) 2976

	SRM 2976 (muscle tissue)		
Elements	Certified values	Measured values	Recovery (%)
Cu	4.02±0.3	4.69±0.5	85.5
Zn	137±13	115±10	84.0
Cd	0.82±0.16	0.66±0.1	80.6
Pb	1.19±0.18	1.03±0.2	86.2

Table (2) and (3) show metal concentrations (µg/g dw) of Cu, Zn, Cd and Pb in the muscles, livers and gills of P. anea and A. maculates and their standard deviations from Kapar. The analysis of variance showed that the mean concentrations of metals in the organs of each fish species were significantly different ($P< 0.05$) in the two species. The mean concentrations of the three tissues indicate different capacities of metal concentrations. The descending order of concentration for Cd, Pb, Cu and Zn was: liver > gills > muscle. Generally, metal accumulation is highest in liver and gills, but it's low in muscles. The results indicate that relatively high concentrations of heavy metals were found in liver and gills of the examined species. Tables 2 and 3 show significant differences in the accumulation levels of metals in the tissues throughout the different seasons in these species. Fishes are able to closely regulate internal Cu concentrations; the highest Cu (55.01µg/g dry weight) concentration was detected in A. maculatus's liver in rainy season and it is lowest level Cu (0.83µg/g dry weight) in muscle of the same fish in dry season. The maximum Zn concentration (555.8µg/g dry weight) was found in A. maculatus's liver in rainy season, while the minimum Zn concentration (17.7µg/g dry weight) in P. anea's muscle in rainy season. Zinc concentrations of the tissues showed a great variation among the fishes. For example, liver and gill Zn concentrations between A. maculates and the P. anea's fish were enormously different.

Table 2. Heavy metals conce ntration (µg metal/g dw) in muscle, liver and gills in two marine fish species in the dry season.

Species	Metal	Tissues	Dry season		WHO*	MFR limits**
			March	April		
A. maculatus	Cu	Muscle	1.68±0.1	0.83±0.02	10	30
		Liver	19.42±1.4	17.94±3.8		
		Gills	1.55±0.1	2.26±0.2		
	Zn	Muscle	22.99±0.2	23.39±0.2	150	100
		Liver	409.8±1.2	356.3±29.5		
		Gills	282.6±4.8	376.2±9.1		
	Cd	Muscle	0.07±0.001	0.04±0.001	0.2	1
		Liver	1.08±0.1	0.23±0.01		
		Gills	0.02±0.003	0.07±0.01		
	Pb	Muscle	0.15±0.004	0.36±0.02	0.2	2
		Liver	0.16±0.0	1.07±0.3		
		Gills	0.27±0.03	0.55±0.1		
P. anea	Cu	Muscle	1.33±0.1	4.38±0.4	10	30
		Liver	19.8±2.4	7.52±0.6		
		Gills	2.89±0.03	1.08±0.1		
	Zn	Muscle	20.62±1.3	32.95±1.5	150	100
		Liver	71.81±7.1	69.97±9.1		
		Gills	115.7±5.5	48.26±5.2		
	Cd	Muscle	0.03±0.001	0.08±0.003	0.2	1
		Liver	0.66±0.002	0.44±0.04		
		Gills	0.16±0.001	0.07±0.04		
	Pb	Muscle	0.41±0.04	0.4±0.04	0.2	2
		Liver	0.96±0.03	0.99±0.01		
		Gills	0.45±0.004	1.73±0.2		

WHO* [20] /MFR limits** [21].

The highest Cd concentration in A. maculates's liver in dry season 1.08µg/g dw, but it was the lowest (0.02µg/g dry wt) in gills of the same species in the same season. Generally, liver samples generally have somewhat higher concentrations than have gill muscle, as Cd tends to accumulate in liver. For Pb maximum concentration was 1.96µg/g dw in P. anea's gills in rainy season; in contrary, the minimum Pb concentration was 0.07µg/g dry wt concentration in A. maculates's muscles in dry season. Lead concentrations in the tissues were higher than the concentrations of cadmium, especially in the muscle and gill.

DISCUSSION

Variation in levels of metals among the fish species is apparent possibly due to differences in metal concentrations in the local environment and chemical characteristics of water from which fishes were caught, ecological needs, metabolism and feeding patterns of fishes, the season in which studies were carried out [22], and also length and weight of the fishes [23] can play a role in accumulation of metals. This study showed that different fish species contained different metal levels in their tissues in different seasons. The levels of metals found in tissues of the A. maculates were generally higher than those found in P. anea throughout the sampling period. The difference in the accumulation of metals in various organs of fishes may be attributed to the proximity to the tissues to the availability of the metals, age and fish species and presence of ligands in the tissues having an affinity to the metal and/or to the role of the tissues in the detoxification process.

Table 3 Mean concentrations (µg metal/g dray wt.) and standard deviations of the metals in the tissues of examined species and the rainy season within the same species.

Species	Metal	Tissues	Rainy season		WHO*	MFR limits**
			Oct	Nov		
A. maculates	Cu	Muscle	3.68±0.7	1.54±0.5	10	30
		Liver	35.43±0.5	55.01±0.1		
		Gills	6.95±0.3	2.21±0.8		
	Zn	Muscle	48.57±0.6	28.12±0.9	150	100
		Liver	555.8±2.4	405.3±37		
		Gills	528.6±6.2	509.3±19.3		
	Cd	Muscle	0.08±0.01	0.09±0.05	0.2	1
		Liver	0.98±0.1	0.46±0.04		
		Gills	0.05±0.01	0.19±0.1		
	Pb	Muscle	0.2±0.02	0.16±0.04	0.2	2
		Liver	0.85±0.01	1.16±0.2		
		Gills	0.24±0.03	0.5±0.1		
P. anea	Cu	Muscle	1.56±0.43	0.94±0.3	10	30
		Liver	15.06±0.4	6.67±0.04		
		Gills	6.52±0.5	1.54±0.2		
	Zn	Muscle	26.32±1.6	17.7±2.7	150	100
		Liver	114.4±2.5	58.30±3.8		
		Gills	60.21±0.4	59.50±2.3		
	Cd	Muscle	0.21±0.03	0.07±0.1	0.2	1
		Liver	0.69±0.05	0.45±0.04		
		Gills	0.21±0.003	0.05±0.1		
	Pb	Muscle	0.17±0.05	0.14±0.1	0.2	2
		Liver	1.07±0.01	1.26±0.1		
		Gills	1.96±0.16	0.79±0.3		

WHO* [20] /MFR limits** [21].

Higher accumulation of trace metals occurred in liver and this may be due to their capacity to accumulate heavy metals brought by blood from other parts including gills and muscles of the body and induce the production of the metal binding protein, metallothionein, that is believed to play a crucial role against the trace metals by binding the metals [24]. [25] found higher concentrations of Cd, Cu and Zn in the liver of fish from an agricultural area. According to [26] and [27], concentrations of heavy metals in gills can be influenced by absorption of metals onto the gill surface, as well as by formation of complexes between the metals and the mucous, which is often impossible to remove them from lamellae prior to the analysis. The highly branched structural organization of the gill and the resultant highly increased surface area, along with the large volume of water passing through the gill surface and the highly vascular physiological state and the relatively small biomass when compared to their surface area make the gill a prime site for trace metals accumulation [27]. Muscle contained the lowest concentrations of trace metals among all the tissues investigated in the present study. Muscle does not come into direct contact with the metals as it is totally covered externally by the skin, that in many ways helps the fish to ward off the penetration of the trace metals and also it is not an active site for detoxification, and therefore transport of trace metals from other tissues to muscle (as in the case of liver and kidneys) does not seem to arise. Results of the currently study show that metal accumulation is highest in liver and gills, while it is low in muscles in all species. This was the case in many fish species, although interspecies differences were shown to accumulate various metals in these tissues [28].

Seasonal changes of metal concentrations in fish species were observed in this study, and this may result from intrinsic factors such as growth cycle reproductive cycle, and from changes in water temperature [29]. Accumulation of bioactive metals like Cu and Zn was actively controlled by the fish through different metabolic processes and the level of accumulations usually independent of ambient concentrations [30]. On the other hand, environmental concentrations affect the accumulation of non-essential toxic elements like Pb [31]. The current study shows that the tissues were generally richest in Zn and Cu, and lowest in Cd and Pb. This different accumulation patterns between the essential elements Zn and Cu on the hand, and Cd and Pb on the other hand might be related to the fact that Zn and Cu are essential for metabolic activities, different ecological needs, metabolism, and feeding pattern [28], and might be as a result of seasonal variation [32]. Higher levels of Pb (in comparison to Cd levels) in tissues are probably due to the motor oil nearly and to the concentrated fishery activities carried out in the region. The currently study is important in terms of understanding metal uptake and accumulation in fish tissues. The physiological role of the tissue in fish metabolism influences the concentration of metals. Some tissues such as the liver and the gills are metabolically active, as compared to low tissues metabolism like muscles [33]. The levels of Cu, Zn, Cd and Pb were determined in the muscle in each species because of their importance for human consumption and also the liver and gills were analyzed since these organs tend to accumulate metals [34]. These organs are also good indicators of chronic exposure to heavy metals because they are the site of metal metabolism. It is well known that heavy metals accumulate in the tissues of aquatic animals, and therefore heavy metals measured in the tissues of aquatic animals can reflect the past exposure to those metals. The liver is often considered a good monitor of water pollution with metals since their concentrations are proportional to those present in the environment. Muscles are poor indicators of low Cu and Zn contamination level [23]. That is also true for most other metals, except for mercury which shows higher affinity to the muscles in comparison to other metals [23]. The liver tissue is highly active in the uptake and storage of heavy metals. It is well known that large amount of metallothionein

induction occurs in the liver tissues of fishes [35]. The gills are uptake site of water borne ions, where metal concentrations increase especially at the beginning of exposure, prior to the entry of metals into the other parts of organism [23]. The levels of the essential metals in the fish samples were higher than those of the non-essential metals.

In spite of muscle is not metabolically active tissue and was a poor indicator of concentration of metals in the fish, it is the main edible fish part and can directly influence human health. For this reason most countries have established toxicological limits for toxic elements in sea food (permissible concentrations). The Malaysian legislation establishes maximum levels for the metals studied, above which human consumption is not permitted;1.0 mg/kg for Cd, 2.0 mg/kg for Pb, 30 mg/kg for Cu and 100 mg/kg for Zn according to Malaysian Food Regulation 1985. Food and Agricultural organization limits for Cd 0.5 mg/kg and Pb 30 mg/kg and 50 mg/kg for Cu and Zn [35]. The concentrations of these metals measured in the muscles of the two fish species studied were generally lower than the levels issued by FAO and Malaysian food regulation.

CONCLUSION

The present study provides information on the distribution of heavy metals in fishes, from the Kapar coastal water. Based on the samples analyzed and metal concentrations found in the edible parts of fishes are not heavily burdened with metals, and the concentrations are below the legal values for fish and fishery products proposed. Zinc concentration was the highest followed by Cu, whereas, Cd was the lowest. Moreover, liver accumulates the highest metal quantity, on the contrary, muscles contain the lowest metal concentration. On the other hand, the results showed that the metal accumulation in rainy season (October and November) was higher than the dry season. During this study significant seasonal differences were recorded in the different tissues of the examined fish species for Cd, Cu, Zn and Pb which may be related to different degree of contamination in different seasons.

REFERENCES

1.EPA – Environmental Protection Agency (2009) Aquatic biodiversity. Available http://www.epa.gov/bioiweb1/aquatic/pollution.html. Accessed 10 July 2010.

2.Cid, B. P., Boia, C., Pombo, L., and Rebelo, E. Determination of trace metals in fish species of the Ria de Aveiro (Portugal) by electrothermal atomic absorption spectrometry. Food Chemistry, 75, 93–100. (2001).

3.Cohen, T., Hee, S. and Ambrose, R. Trace metals in fish and invertebrates of three California coastal wetlands. Marine Pollution Bulletin, 42: 232–242. (2001).

4. Canl, M., and Atl, G. The relationships between heavy metal (Cd, Cr, Cu, Fe, Pb, Zn) levels and thesize of six Mediterranean fish species. Environmental Pollution, 121(1): 129–136. (2003).

5.Irwandi, J. and Farida, O. “Mineral and heavy metal contents of marine fin fish in Langkawi island, Malaysia,” International Food Research Journal, vol. 16 (1): 105–112. (2009).

6.Kamaruzzaman, B. Y., Rina, Z., Akbar john, B. and Jalal, K. C. A. Heavy metals accumulation in commercially important fishes of south west Malaysian coast. Research Journal of Environmental Sciences, 5(6): 595-602. (2011).

7.Chen, D., Zhang, M. and Shrestha, S. Compositional characteristics and nutritional quality of Chinese mitten carb (Eriocheir sinensis). Food chemstiry. 103 (4): 1343-1349. (2006).

8.Zalloua, P. A., Hsua, Y., Terwedowa, H., Zangc, T., Genfu Tang, D.W. and Li, Z. Impact of seafood and fruit consumption on bone mineral density. Maturitas, 56: 1–11. (2007)

9.Tuzen, M. and Soylak, M. Determination of trace metals in canned fish marketed in Turkey. Food chemistry, 101: 1378–1382. (2007).

10.Turkmen, M., Turkmen, A., Tepe, Y., Tore, Y., and Ates, A. Determination of metals in fish species from Aegean and Mediterranean Sea. Food chemistry,113: 233–237. (2009).
11.Ptashynski, M. D., Pedlar, R. M., Evans, R. E., Baron, C. L. and Klaverkamp, J. F. Toxicology of dietary nickel in lake white fish (Coregonus clupeaformis). Aquatic Toxicology, 58(3–4): 229–235. (2002).
12.W. H. Toxic responses of the gill. In: Schlenk, D., Benson, W. H. (Eds.), Target Organ Toxicity in Marine and Freshwater Teleosts. Taylor and Francis, London, pp. 1–89. (2001).
13.Bury, N. R., Walker, P. A. and Glover, C. N. Nutritive metal uptake in teleost fish. Journal of Experimental Biology, 206 (11), 23. (2003).
14.Uysal, K., Emre, Y. and Kose, E. The determination of heavy metal accumulation ratios in muscle, skin and gills of some migratory fish species by inductively coupled plasma-optical emission spectrometry (ICP-OES) in Beymelek Lagoon (Antalya/Turkey). Microchem., 90: 67–70. (2008).
15.Camara, F., Amaro, M. A., Barbera, R. and Clemente, G. "Bioaccessibility of minerals in school meals: Comparision between dialysis and solubility methods." Food Chemistry, 92: 481–489. (2005).
16.Erdoğrul, Z. and Ates, D. A. Determination of cadmium and copper in fish samples from Sir and Menzelet dam lake Kahramanmaras, Turkey. Environ. Monit. Assess., 117:281–290. (2006).
17.Zhang, I. and Wong, M. H. Environmental mercury contamination in China: Sources and impacts. Environmental International, 33: 108–121. (2007).
18.Abdullah, A. R., Tahir, N. M., Loong, T. S., Hoque, T. M. and Sulaiman, A. H. The accumulation in commercially important fishes of south west Malaysian coast. Research Journal of Environmental Sciences, 5 (6): 595-602. (1999).
19.Eng, C. T., Paw, J. N. and Guarin, F. Y. "The environmental impact of aquaculture and the effects of pollution on coastal aquaculture development in southeast Asia." Marine Pollution Bulletin, 20: 335–343. (1989).
20.World Health Organization. "Heavy metals-environmental aspects," Environment Health Criteria , no. 85, World Health Organization, Geneva, Switzerland. (1989).
21.FAO/WHO. Joint FAO/WHO food standards programe codex committee on contaminants in food, fifth. Session Pp 64-89. (2011).
22.Rauf, A., Javed, M. and Ubaidullah, M. Heavy metal levels in three major carps (Catla catla, Labeo rohita and Cirrhina mrigala) from the River Ravi, Pakistan. Pakistan Veternery Journal, 29(1) 24–26. (2009).
23.Jezierska, B. and Witeska, M. Metal toxicity to fish. University of Podlasie, Monografie. No. 42. .(2001).
24.Iwegbue, C. M. A. Heavy metal composition of livers and kidneys of cattle from southern Nigeria. Veterinarski Archiv., 78(5): 401-410. (2008).
25.Köck, G., Triendl, M. and Hofer, R. Seasonal patterns of Metal accumulation in arctic char (Salvelinus alpinus) from an oligotrophic Alpine Lake related to temperature. Canadian Journal of Fisheries and Aquatic Sciences., 53(4): 780-786. (1996).
26.Dural, M., Goksu, M. Z. L. Ozak, A. A. and Derici, B. Bioaccumulation of some heavy metals in different tissues of Dicentrarchus labrax L, 1758, Sparusa aurata L, 1758, and Mugil cephalus L, 1758 from the Camlik Lagoon of the eastern coast of Mediterranean (Turkey). Environ. Monit. Assess., 118: 65-74. (2006).
27.Erdoğrul, O. and Erbilir, F. Heavy metal and trace elements in various fish samples from Sir Dam Lake, Kahramanmaraş, Turkey, Environ. Monit. Assess. 130, 373–379. (2007).
28.Dural, M., Goksu, M. Z. L. and Ozak, A. A. Investigation of heavy metal levels in economically important fish species captured from the Tuzla lagoon. Food chemistry, 27: 521–526. (2010).
29.Chatterjee, S., Chattopadhya, B. and Mukhopadhaya, S. K. Trace metal distribution in tissues of cichlids (Oreochromis niloticus and O. mossambicus) collected from wastewater-fed fish ponds in east Calcutta wetlands, a Ramsar site. Acta Chthyologica Et Piscatoria, 36(2), 119–125. (2006).
30.Pattee, O. H. and Pain, D. J. Lead in the environment. In: D. J. Hoffman, B. A., Rattner, G. A Burton J. R. and Cairns, J. (Eds.), Handbook of Ecotoxicology (2nd ed., pp. 373–408). Boca

Raton, Florida. (2003).
31.Deram A., Denayer, F. O., Petit, D., and Van Haluwyn, C. Seasonal variations of cadmium and zinc in Arrhenatherum elatius, a perennial grass species from highly contaminated soils. Environ. Pollut. 140: 62– 70. (2006).
32.Ploetz, D. M., Fitts, B. E. and Rice, T. M. Differential accumulation of heavy metals in muscle and liver of a marine fish, (King Mackerel, Scomber omorus Cavalla Cuvier) from the northern gulf of Mexico, USA. Bulletin of Environmental Contamination and Toxicology 78(2): 134-137. (2007).
33.Marcovecchio, J. E., Moreno, V. J. and Pérez, A. Metal accumulation in tissues of sharks from the Bahía Blanca Estuary, Argentina. Marine Environmental Research., 31(4): 263-274. (1991).
34.Langston, W. J. Toxic effects of metals and the incidence of metal pollution in marine ecosystems. In: Heavy metals in the marine environment. Furness, R. W. And Rainbow, P. S. CRC press, Boca Raton, Florida, United States of America 143-182. (1990).
35.Food and Agriculture Organization (FAO). “Compilation of legal limits for hazardous substances in fish and fishery products,” FAO Fishery Circular, 464: 5–10. (1983).

Emergence of CTX-M Gene Among ESBL Positive E.Coli Isolates form UTI Outpatients at Benghazi

Fauzia Rajab El-Garbulli[1], Muna Mohammed Buzayan[2*], and Najla Mathlouthi[3]

[1]Department of Botany, Faculty of Science, BenghaziUniversity, Benghazi, Libya.
[2*]Kaser Ahmed Hospital,Misurata, Libya.
[3]Faculty of Sciences of Tunis, Laboratory Microorganisms and Active Biomolecules, University of Tunis El Manar, 2092 Tunis, Tunisia.
*Corresponding author. E-mail: fauzia.r511@yahoo.com

Abstract—**Background & Objective**: The detection of clinical Escherichia coli producing extended-spectrum b-lactamases (ESBLs) are increasingly important cause of community acquired infection worldwide. The aim of this study was to investigating the presence of bla OXA, bla TEM, bla SHV and bla CTX-M genes among ESBL-producing E. coli isolated from Urinary Tract Infection (UTI) out-patients in Benghazi Center of Infectious Disease and Immunity (BCIDI).

Methodology: 40 E. coli isolates were collected from UTI outpatients at the Benghazi Center of Infectious Disease and Immunity during the period of 2011 to 2012. The antibiotic susceptibility of E. coli isolates were determined by disc-diffusion method as accordance with British society for antimicrobial chemotherapy (BSAC) [5] and by using the Phoenix Automated Microbiology System (Becton Dickinson, USA). ESBL production was screened by using the double disk synergy test. ESBLs coding genes (bla OXA, bla TEM, bla SHV and bla CTX-M (CTX-M universal, CTX-M-3G)) were identified by PCR.

Results: 16 ESBL-producing E. coli were identified among the E. coli isolates. Molecular investigated isolates (17) were negative for bla TEM, bla SHV, bla OXA-1 genes, three strains were positive for bla CTX-M-3G gene , six strains were carrying each of bla CTX-M-U and bla CTX-M-3G genes, three strains was positive for bla CTX-M-U gene and five strains were negative for CTX-M-U and CTX-M-3G type b-lactamases.

Conclusions: The emergence of CTX-M gene among ESBL positive E. coli isolates from UTI outpatients at Benghazi were documented; however, further studies are required to study the epidemiology and genetic characterization of other CTX-M types of ESBLs.

Key words: urinary tract infection; ESBL-producing E. coli; CTX-M-gene.

INTRODUCTION

B-lactamase is enzyme produced by micro-organism that hydrolyse b-lactam molecules. It is the most common B-lactam resistance mechanisms that contribute wide spread resistance among gram negative bacteria [6].

B-lactamase differ from each other in substrate profile and inhibitor profile.They also differ in a composition of hydrolytic parts of these enzymes [7]. The evolution of ESBL OXA-type -lactamases from parent enzymes with narrower spectra has many parallels with the evolution of SHV- and TEM-type ESBLs (Paterson& Bonomo, 2005).

ESBLs were initially derived from TEM and SHV and were essentially restricted to health care facilities that have evolved from parent enzymes, such as TEM-1, TEM-2, and SHV-1 [19 - 4]

B- lactamases resistance is expressed chromosomally or plasmid borne. The ability of E. coli to acquire and transfer anti- microbial resistance genes is considered. ESBLs-producing E. coli isolates where detected in hospitals as well as the community [20-19]

CTX-M enzymes were reported in Germany and Argentina in 1989 and since the increase of these strains have been reported in different geographical areas and they have become the most prevalent ESBLs [8]. Detection of CTX-M by molecular methods in ESBL-producing bacteria and their pattern of antimicrobial resistance is important for infection control. It can provide useful information about its epidemiology and help in rational antimicrobial therapy [14 -12].

Sofor 4 groups of B-lactamase have been identified based on substrate specification pencillinase, Amp c- type cephalosporinase, ESBLs and carbapenemase. In the present study, we investigate the occurrence of ESBLs genes in UTI patients using phenotype and molecular methods.

MATERIALS AND METHODS

Bacterial strains:

40 E. coli samples were isolated from uropathogens of UTI outpatient at BCIDI during the period of 2011 to 2012. They were identified with Phoenix Automated Microbiology System (Becton Dickinson, USA) (BD). All identified isolates were stored in brain heart infusion (BHI) broth containing 20% glycerol at -20^0C.

Antimicrobial susceptibility testing:

Antimicrobial susceptibility testing for E. coli isolates were determinedby using the Phoenix Automated Microbiology System.The panel (NMIC/IC-94) for gram negative bacteria was containing amikacin, amoxicillin/clavulanate, ampicillin, aztreonam, cefepime, ceftazidime, ceftriaxone, cefuroxime, cefoxitin,cephalothin,ciprofloxacin, ertapenem, gentamicin, imipenem, levofloxacin, meropenem, nitrofurantoin, piperacillin/tazobactam, trimethoprim/sulfamethoxazole .The results are also interpretedthrough a computerised system.

Phenotype method for ESBL:

Phenotypic detection of ESBL production in isolated samples was performed by their susceptibility to the third generation cephalosporin's [ceftazidime (30 g), cefotaxime (30 g) and ceftriaxone (30 g)] and aztreonam (30 g)(Oxoid Ltd., Cambridge, UK) by using Kirby Bauer disk diffusion method. The diameters of the zones of inhibition were measured according to the British society for antimicrobial chemotherapy [5] recommendations. The isolates that showed resistance to at least one of the four antibiotics were tested for ESBL production by the double-disk synergy test (DDST method) as described by [15].

Detection of beta-lactamase genes:

Molecular characterization of uropathogenic E.coli was investigated only on 17of 40 UTI samples. Total DNA extraction was performed Laboratory of Microorganisms and Active Biomolecules, Faculty of Sciences of Tunis, University of Tunis El Manar, Tunisia.

Molecular detection of gene coding for the TEM, SHV, OXA-1, CTX-M (CTX-M universal) andCTX-M3G(CTX-M-1 group)type beta-lactamases was performed by using polymerase chain reaction (PCR) described previously in [16-11] The oligonucleotide primer sets specific for the β-lactamase genes and conditions of amplification of these genes in isolated genomic DNA samples used in PCR assays are listed in Table1. PCR products were analysed by 1% agarose gel electrophoresis and photo- documented after stained with ethidium bromide.

Table 1: primers sequences and condition used for the polymerase chain reaction (PCR) amplification of different B-lactamase genes.

PCR Target	**Primer name**	**Primer sequence (5′–3′)**	**amplicon size**	**Reference**	**Conditions amplification**
BlaTEM	TEM-F TEM-R	F: TTCTTGAAGACGAAAGGGC R: CGCTCAGTGGAACGAAAAC	1150pb	[16]	94°C 3min 1 cycle 94°C 1min 60°C 1min 30cycle 72°C 1min 72°C 5min 1 cycle
bla SHV	SHV-F SHV-R	F: CACTCAAGGATGTATTGTG R: TTAGCGTTGCCAGTGCTCG	885pb	[16]	96°C 15s 1 cycle 96°C 15s 52°C 15s 24cycle 72°C 2min 72°C 3min 1 cycle
bla OXA	OXA-1 F OXA-1 R	F:ACACAATACATATCAACTTCGC R: TGTGTTTAGAATGGTGATC	813pb	[16]	96°C 5min 1 cycle 96°C 1 min 61°C 1min 35cycle 72°C 2min 72°C 10min 1 cycle
BlaCTX-M (CTX-M universal)	CTX-M-U-F CTX-M-U-R	F:CGATGTGCAGTACCAGTAA R:TTAGTGACCAGAATCAGCGG	454 pb	**[11]**	94°C 5min 1 cycle 94°C 30s 52°C 30s 35cycle 72°C 1min 72°C 5min 1 cycle
bla CTX-M-3G(CTX-M-1 group)	CTX-M3G-F CTX-M3G-R	F:GTTACAATGTGTGAGAAGCAG R: CGTTTCCGCTATTACAAAC	1041pb	[16]	94°C 7min 1 cycle 94°C 50s 50°C 40s 35cycle 68°C 1min 68°C 5min 1 cycle

RESULTS

Antimicrobial susceptibility of clinical isolates:

ESBL-producing E. coli were high resistant to ampicillin (94.1%), amxocillin / clavulanate (82.4%), ciprofloxacin, ceftriaxone, levofloxacin, (76.5%), cefotaxime, ceftazidime, aztreonam, cefuroxime (70.6%), trimethoprim/sulfamethoxazole, cefepime (64.7%). All ESBL-producing E. coli were high sensitive to imipenem, meropenem and amikacin (100%), nitrofurantoin (94.1%), ertapenem (94.1%), %), cefoxitin (88.2%), piperacillin-tazobactam (82.4 %) and gentamycin (76.5%), Figure 1.

Characterization of beta lactamases:

Molecular detection of 16 ESBL-producing E. coli were isolated from UTI outpatient were confirmed by phenotype methods using the double disk synergy test (Fig. 2) .Only one strain was non-ESBL strain (Table 2).

All isolates were negative for bla TEM, bla SHV, bla OXA-1 genes, three strains were positive for blaCTX-M-3G gene , six strains were carrying each of bla CTX-M-U and bla CTX-M-3G genes , three strains was positive for bla CTX-M-U gene and five strains were negative for CTX-M-U and CTX-M-3G type b-lactamases. Table 2 shows also presence of GTX-M-3G in sample 15 which was ESBL negative by phenotype methods, (fig.3 and fig.4).

TABLE 2. Antimicrobial susceptibility profiles and bla genes detected by PCR in sixteen phenotypic positive ESBL-producing E. coli and one phenotypically negative sample Cefotaxime (CTX), ceftazidime (CAZ), cefuroxime (CXM), ceftriaxone (CRO), aztreonam (ATM), amoxicillin/clavulanate (AMC),cefepime (FEP), imipenem (IPM), cefoxitin (FOX), gentamicin (CN), ampicillin (AMP), ciprofloxacin (CIP), ertapenem (ETP), levofloxacin (LEV), nitrofurantoin (F), trimethoprim/sulfamethoxazole (STX).

No. of E. coli isolates	Antibiotics									Detected β-lactamase (bla types)	Resistance phenotype to non β-lactam antibiotics
	CTX	CAZ	CXM	CRO	ATM	AMC	FEP	IPM	FOX		
1	R	R	R	R	R	R	I	S	I	CTX-M-U,CTX-M-3G	AMP, SXT, CN
2	R	R	R	R	R	R	R	S	R		AMP,CIP,LEV,SXT
3	R	R	R	R	R	R	I	S	R	CTX-M-U,CTX-M-3G	AMP,CIP,LEV,SXT
4	R	R	R	R	R	R	R	S	S	CTX-M-U,CTX-M-3G	AMP,CIP,LEV,CN
5	R	R	R	R	R	R	R	S	S	CTX-M-U,CTX-M-3G	AMP,CIP,LEV,SXT,CN
6	R	R	R	R	R	R	R	S	S	CTX-M-U,CTX-M-3G	AMP, SXT
7	I	I	I	S	S	I	S	S	I		AMP,CIP,LEV,SXT
8	R	R	R	R	R	R	R	S	S	CTX-M-U, CTX-M-3G	AMP
9	R	R	R	R	R	R	R	S	S		AMP,CIP,LEV, SXT
10	R	R	R	R	R	R	R	S	S		AMP,CIP,LEV
11	S	S	I	R	S	R	R	S	S		AMP,CIP,LEV,SXT
12	R	R	R	R	R	R	R	S	S	CTX-M-U	AMP, CIP, CN,SXT
13	R	R	R	R	R	R	R	S	S	CTX-M-3G	AMP, CIP,CEF,LEV
14	R	R	R	R	R	R	R	S	S	CTX-M-U	AMP
15	S	S	S	S	S	I	S	S	S	CTX-M-3G	AMP,CIP,LEV,SXT,F
16	I	S	S	S	S	R	S	S	S	CTX-M-U	AMP,CIP,LEV,SXT
17	I	S	S	S	S	S	S	S	S	CTX-M-3G	CIP,LEV

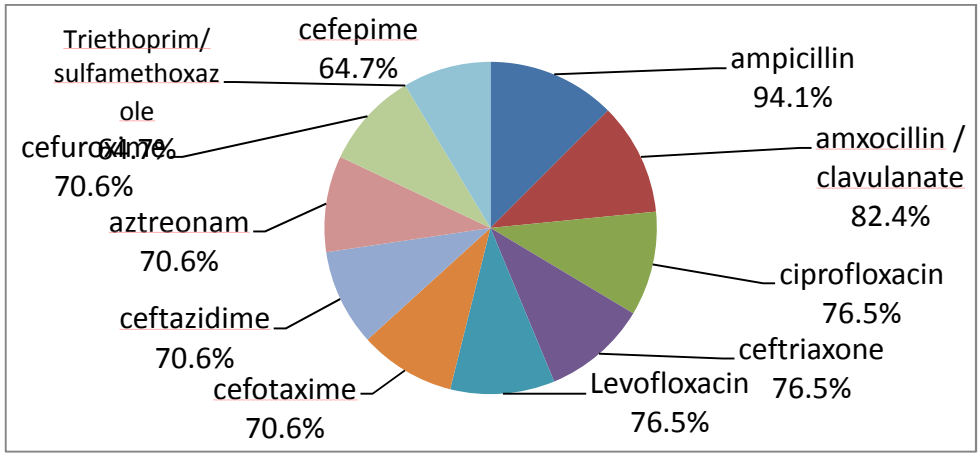

Figure 1: Susceptibility of ESBL-producing E. coli isolates.

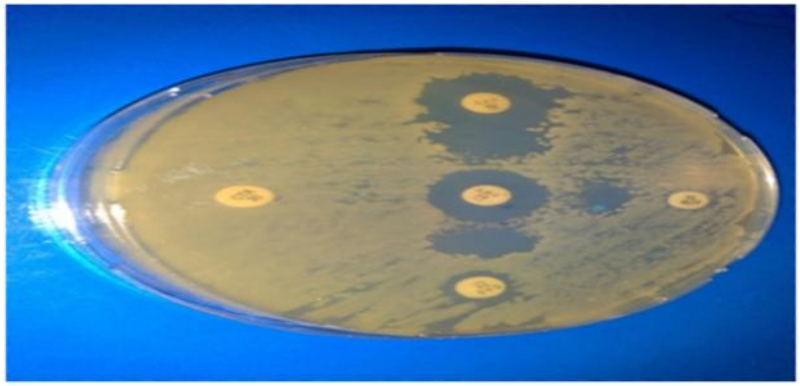

Figure 2: ESBL-producing E. coli were confirmed by using the double disk synergy test on Muller Hinton agar

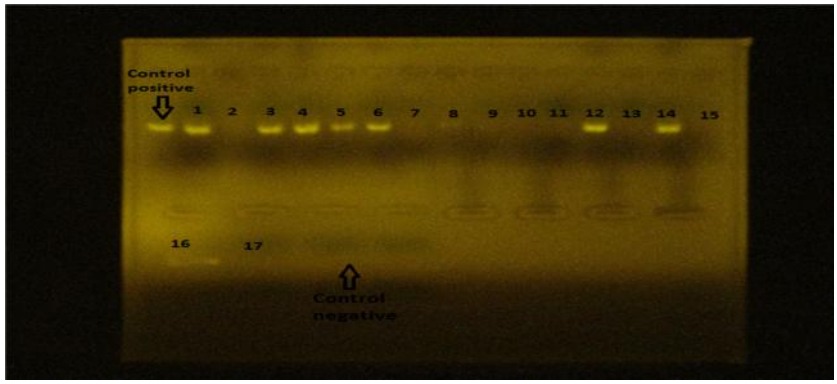

Figure 3: Result of the PCR screening test of E. coli for bal genes using CTX –M-U primer. Line 1: positive control for CTX-M-U gene, Line 2 – 17 PCR product of ESBL-producing E. coli isolated samples , Line 18: negative control for CTX-M-U gene

Figure4:Result of the PCR screening for bal genes using CTX –M-3G primer
Line 1: positive control for CTX-M-3G gene, Line 2 - 17 PCR product of ESBL-producing E. coli isolated samples , Line 18: negative control for CTX-M-3G gene

DISCUSSION

The aim of this study was to determine the prevalence and characterize ESBL producers among uropathobens E. coli collected from UTI outpatients in BCIDI. The indicate confirm the high prevalence of CTX-M-3G, CTX-M-U gene (35.3%), CTX-M-U gene (17.6%) andCTX-M-3G gene (17.6%), while the prevalence of other SHV, TEM and OXA-1 genes was absent (Table 2) Bourjilat et al. [3] in Moroccoand Ahmed [1] have studied Seven strains of E. coli producers of ESBLs among the 535 E. coli isolates, he found that (6/7) of the strains were carriers of the gene CTX-M, Two strains were high prevalence was 6/7 observed by --- and Sudan (Coque et al, 2008) carrying TEM gene in combination with CTX-M-15 or SHV-5. In Khartoum, Sudan, the prevalence of E. coli producers of ESBL has also increased with a predominance of CTX-M (71.4%), TEM and SHV were 55.1%, 6.1% respectively [1]. Recently, the predominant ESBL genotype in E. coli in Europe has changed from TEM / SHV to CTX-M [26].

Yumuk [26] reported that CTX-M is common among the ESBL producing E. coli isolates obtained from community acquired UTIs in Izmir, Turkey. In Norway the CTX-M is the ESBL enzyme most frequently found in E. coli [23]. Vidhya and Sudha [24] and Jouini et al. [16] showed that there was a high prevalence of the bla CTX-M gene (80%) among ESBL positive E. coli isolates from the UTI patients using CTX-M primer in Coimbatore, South India.

The prevalence and distribution of CTX-M enzymes data are limited in Benghazi, there is no data comparing CTX-M, TEM and SHV type ESBLs in hospitalized and outpatients. In this study, the rate of CTX-M type ESBL producing E. coli was found to be quite high as 66.7 %. Although, we do not know the exact prevalence of these enzymes and factors influencing their high rate of ESBL producing strain in Benghazi, the current study suggests that CTX-M-producers have already begun to disseminate throughout Benghazi.

The presence of ESBL enzyme type M was in arrangement with synergy test results. In some cases such as isolates 17 PCR product indicate the presence of CTX-M3G gene but this isolates was sensitive to most studied antibiotic.tje negative phenotype results of this isolates maybe due to site directed mutagenesis [21] This data shows that molecular detection of ELSB is more sensitive than using phenotype method.

In recent years; the general susceptibility pattern of ESBL producer strains to antibiotics has decreased in many countries [13-; 10]. The ESBL producers in this study were high resistance to ampicillin, ciprofloxacin, levofloxacin, amoxicillin/ clavulanic acid, trimethoprim/ sulfamethoxazole which is of great concern because these the drugs of choice for first –line empiric treatment of both community and hospital acquired UTIs. Among oral agents licensed for treatment of urinary tract infection (UTI), only nitrofurantoin was generally active. The occurrence of CTX-M enzymes represents treatment problems in the community [25].

CONCLUSION

In our study, CTX-M type of ELSB was clearly the most prevalent enzyme among the community acquired E. coli causing UTIs in Benghazi. The results of antibiotic susceptibility revealed a high rates of resistance against the fluoroquinolones which are widely used in treatment of the urinary tract infections in Benghazi. The usage of carbapenems will still be suitable for a successful treatment of infections by E .coli. After carbapenems, aminoglycosides can be considered as the second most effective agent.

The emergence of CTXM from Benghazi is alarming; however, further studies are required to be conducted with the purpose of studying the epidemiology and genetic characterization of CTX-M types of ESBLs.

REFERENCES

1. Ahmed O, Omar A, Asghar A and Elhassan M. Prevalence of TEM, SHV and CTX-M genes in Escherichia coli and Klebsiella spp Urinary Isolates from Sudan with confirmed ESBL phenotype. Life Science Journal 2013;10(2):191-195.
2. Bonnet R. Growing group of extended-spectrum b-lactamases: the CTX-M enzymes. Antimicrob Agents Chemother 2004; 48: 1–14.
3. Bourjilat F, Bouchrif B, Dersi N, Claude J, Amarouch H, Timinouni M. Emergence of extended-spectrum beta-lactamase-producing Escherichia coli in community-acquired urinary infections in Casablanca, Morocco. J Infect DevCtries 2011; 5(12):850-855.
4. Bradford PA. Extended-spectrum beta-lactamases in the 21st century: characterization, epidemiology, and detection of this important resistance threat. ClinMicrobiol Rev 2001; 14:933–951.
5. British society for antimicrobial chemotherapy (BSAC). BSAC Methods for Antimicrobial Susceptibility Testing. Version 10.2 May 2011.
6. Bush K, Jacoby G.A. Updated functional classification of beta lactamase. Antimicrob agent chemother 2010; 54, 969-976.
7. Bush K. The coming of age antibiotic discovery and therapuaticalue. Ann NY AcadSci 2010; 1212, 1-4.

8. CantÓn R, Novais A, Valverde A, Machado E, Peixe L, Baquero F and Coque T.M. Prevalence and spread of extended-spectrum b-lactamase-producing Enterobacteriaceae in Europe. ClinMicrobiol Infect 2008; 14 (Suppl. 1): 144–153.
9. Coque TM, Baquero F, Canton R: Increasing prevalence of ESBL producing Enterobacteriaceae in Europe. Eurosurveillance 2008, 13 (47).
10. Daoud Z, Hakime N: Prevalence and susceptibility patterns of extended-spectrum ß-lactamase producing Escherichia coli and Klebsiella pneumoniae in a general university hospital in Beirut, Lebanon. Revista Espanola de Quimioterapia 2003, 16:233-238.
11. Eckert C, Gautier V, Saladin-Allard M, Hidri N, Verdet C, Ould-Hocine Z, Barnaud G, Delisle F, Rossier A, Lambert T, Philippon A, and Arlet G. Dissemination of CTX-M-Typeβ-Lactamases among Clinical Isolates of Enterobacteriaceae in Paris, France. Antimicrobial agents and chemotherapy 2004: 1249–1255.
12. Garrec H , Drieux-Rouzet L, Golmard J, Jarlier V, and Robert J. Comparison of Nine Phenotypic Methods for Detection of Extended-Spectrum β-Lactamase Production by Enterobacteriaceae. J clinmicrobiol2011: 1048–1057.
13. Hamouche E, SarkisDK : Evolution of susceptibility to antibiotics of Escherichia coli, Klebsiella pneumoniae, Pseudomonas aeruginosa and Acinetobacter baumanii, in a University Hospital Center of Beirut between 2005 and 2009. PatholBiol (Paris) 2011.
14. Jain A &Mondal R. TEM and SHX genes in extended spectrum β-lactamase producing Klebsiella species and their antimicrobial resistance pattern. Indian J. Med. Res 2008;128: 759-764.
15. Jarlier V, Nicolas MH, Fournier G &Philippon A. 1988. Extended Broad-Spectrum β-Lactamases Conferring Transferable Resistance to Newerβ -Lactam Agents in Enterobacteriaceae: Hospital Prevalence and Susceptibility Patterns. Rev. Infect. Dis. 10: 867-878.
16. Jouini A, Vinue´L , Ben Slama K, Sáenz Y, Klibi N, Hammami S, Boudabous A and Torres C. Characterization of CTX-M and SHV extended-spectrum β-lactamases and associated resistance genes in Escherichia coli strains of food samples in Tunisia. Journal of Antimicrobial Chemotherapy 2007;60: 1137–1141.
17. Lartigue M, Zinsius C, Wenger A, Bille J, Poirel L, and Nordmann P. Extended-Spectrum β-Lactamases of the CTX-M Type Now in Switzerland. Antimicrobial Agents and Chemotherapy, 2007: 2855–2860.
18. Paterson DL and Bonomo RA. Extended-Spectrum β-Lactamases: a Clinical Update. ClinMicrobiolRevi 2005; 657–686.
19. Pitout JD, Laupland KB. Extended-spectrum beta-lactamase-producing Enterobacteriaceae: an emerging public-health concern. Lancet Infect Dis 2008.
20. Quinteros M, Radice M, Gardella N, Rodringuez MM, Costa N, Korbenfeld D, Couto E, Gutkind G. Extended- spectrum B-lactamase in Enterobacteriaceae in Buenos Aires Argentina, public hospitals. Antimicrob Agents Chemother 2003; 47, 2864-2867.
21. Randegger CC, Keller A, Irla M, Wada A and Hächler H. Contribution of natural amino acid substitutions in SHV extended-spectrum β-lactamases to resistance against various β-lactams. Antimicrob. Agents Chemother. 2000, 44 ;(10):2759-2763.
22. Smet A, Martel A, Persoons D, Dewulf J, Heyndrickx M, Claeys G, Lontie M, Meensel B, Herman L, Haesebrouck F, and Butaye P. Characterization of

Extended-Spectrum β-Lactamase Produced by Escherichia coli Isolated from Hospitalized and Nonhospitalized Patients: Emergence of CTX-M-15-Producing Strains Causing Urinary Tract Infections. Microbial Drug Resistance 2010; Vol.16, No. (2):129-134.

23. Tofteland S, Haldorsen B, Dahl KH, Simonsen GS, Steinbakk M, Walsh TR: Effects of phenotype and genotype on methods for detection of extended-spectrum ß-lactamase producing clinical isolates of Escherichia coli and Klebsiella pneumoniae in Norway. J ClinMicrobiol 2007, 45:199-205.
24. Vidhya N, Sudha S.S. Prevalence of Bla CTX-M extended spectrum Beta-Lactamase gene in uropathogenic Escherichia coli. World journal of pharmacy and pharmaceutical sciences 2013. Vol. 2, Issue 6, 6548-6558.
25. Woodford N, Ward M.E, Kaufmann M.E, Turton J, Fagan E.J, James D,Johnson A.P, Pike R, Warner M, Cheasty T, Pearson A, Harry S, Leach J.B,Loughrey A, Lowes J.A, Warren R.E and M. Livermore D.M. Community and hospital spread of Escherichia coliproducingCTX-M extended-spectrum b-lactamases in the UK. Journal of Antimicrobial Chemotherapy 2004; 54: 735–743.
26. Yumuk Z, Afacan G, Nicolas-Chanoine MH, Sotto A, Lavigne JP. Turkey: a further country concerned by community-acquired Escherichia coli clone O25-ST131 producing CTX-M-15. J. Antimicrob. Chemother2008 ; 62(2):284-288.

Hot Particle Dosimetry, Part-III: Enhanced EGSnrcMP Dose Estimates over EGS4 for a ^{106}Ru/Rh Hot Particle, Compared to Measurements using Imaging Photon Detector, RadioChromic Dye Film and Extrapolation Chamber

[*]I. E. Othman, [**]M. Amer and [*]A. Alsariti

[*]Physics Department, Faculty of Science, Misurata University
[**]Biomedical Engeneering Department, Libyan Academy

iemothman@gmail.com

Abstract— Hot particle of ^{106}Ru/Rh is considered as high energy beta emitter with E_{max}=3.54 MeV. Dose comparisons around ^{60}Co (E_{max}=0.318 MeV) and ^{170}Tm (E_{max}=0.986 MeV) model hot particles between electron gamma shower EGS4 and each of radiochromic dye film (RDF) and thermoluminescence imaging photon detector IPD techniques were previously done. In this work, dose measurements were extended to high energy beta ^{106}Ru/Rh model hot particle using the more conventional measurement techniques, extrapolation chamber (ECH) and (RDF) and simulated using the new Monte Carlo EGSnrcMP code. The IPD with novel thin clear fused quartz dosemeter CFQ (200 µm thick) was also used. For EGS4, the agreement between the measurements and code predictions is reasonably good. Overall ratios of 1.31 ± 0.39, 1.02 ± 0.19 and 1.12 ± 0.07 for ECH, RDF(GafChromic) and IPD(CFQ) techniques, respectively show some evidence of a possible systematic tendency for EGS4 code to overestimate the measurements for the higher energy sources, especially at small averaging areas and underestimate the doses for large areas. This overestimate is about 90% for EGS4 and about 30% for EGSnrcMP. On the other hand, the underestimate is about 19% for EGS4 and about 9% for EGSnrcMP. In the area range 0.5-5.0 cm^2, importance of current radiological protection criteria, the agreement is improved, compared to ^{60}Co and ^{170}Tm model hot particles, with overall ratio of 1.03 ± 0.03 for CFQ compared to 0.87±0.02 and 0.85±0.04 for ECH and RDF, respectively. In the case of the recommended skin dose averaged over 1 cm at 7 mg cm^{-2}, the ratio EGS/IPD is about 1.01. For the dose distribution, in general, using EGSnrcMP, the agreement is reasonably good (9%) compared to 15% for EGS4

Keywords- Hot Particles, Radiation Dosimetry, EGSnrc, Monte Carlo, Imaging Photon Detector, Extrapolation Chamber, RadioChromic Dye Film, Non-uniform Dose Distribution, Skin Dosimetry. Radiological Protection.

INTRODUCTION

The evaluation of the hazard, posed by very small radioactive particles (<1 mm diameter), has become known as the "hot particle problem" [1]. During the late 1960's the term hot particle came into prominent usage when the carcinogenic effects produced in the lung by

discrete small particles containing alpha emitting radio-nuclides, particularly ^{239}Pu, were being postulated by Geesaman 1968 [2] and Dean and Langham 1969 [3] to be several orders of magnitude greater than that produced by uniform irradiation to the same dose. The term "hot particle" appears to have arisen from the problem of comparing the effect of a uniform external gamma ray dose with that of the extremely non-uniform pattern of dose produced by the deposition of a number of discrete beta particle sources in the lung epithelium of an unprotected man immersed in a cloud of radioactive fallout on a nuclear battlefield [4].

Hot particle hazards exist in the nuclear power industry, in the processing of radioactive ore, in medical, industrial and research applications of radioactive isotopes and around accelerators. The two primary types of hot particles are from failed nuclear fuel and from neutron activated particles produced by corrosion and wear [5-8].

In the case of external exposure to hot particles, the measurement of dose is problematic and particularly demanding. The dosimetric problem arises primarily from the rapid attenuation of the beta radiation with the tissue depth. This leads to a strong dependence of biological response on the beta ray energy. In the case of the skin, if it is irradiated by hot particles at very short distances, the spatial distribution of dose would be extremely non uniform for geometrical reasons. The measurement of an absorbed dose, over some specific area, requires a detector to have a wide dynamic range and to preferably have a linear response over this range. An equally important difficulty is the need to measure doses over very thin layers, such as that of basal cells in the skin which are within 20-100 μm of the skin surface on somebody sites. To simulate such volumes, the detector must be extremely thin, with consequent reduction in sensitivity. For general radiological protection applications the International Commission on Radiological Protection ICRP recommends the use of a depth of 70 μm and the dose is averaged over an area of $1cm^2$ [9-10]

Measurements and calculations of beta spectra and dose distributions around ^{60}Co (E_{max}=0.318MeV) and ^{170}Tm (E_{max}=0.986 MeV) model hot particles have been previously studied [11-18]. The measurements and calculations are extended in this work to the higher energy beta emitter $^{106}Ru/Rh$ (E_{max}=3.54 MeV) following construction of a further model hot particle (ERU1). An imaging photon detector (IPD) and the Monte Carlo code EGS4 (dosrz) were used to estimate the spatial and depth dose distributions around ERU1. The more conventional measurement techniques, extrapolation chamber (ECH) and radiochromic dye film (RDF) were used for comparisons with the IPD and EGS4 measurements for a $^{106}Ru/Rh$ model hot particle. The new EGSnrcMP Monte Carlo code system were used for comparisons with all above techniques.

MATERIALS AND METHODS

Basic design of ^{106}Ru/Rh source

While the active elements in the previous ^{60}Co and ^{170}Tm model hot particles were produced by neutron activation of well-defined microscopic forms, prepared in house, the higher energy ^{106}Ru/Rh parent/daughter combination is only obtainable by chemical separation from a fission product mixture. The ERU1 source was therefore constructed by incorporating a commercially available electrodeposited Ru disc source encapsulated in a stainless steel needle into the standard aluminium mount used in the ^{60}Co and ^{170}Tm model hot particles. Although this approach may be less than ideal, in that the geometry of the active element cannot be so readily verified, the higher energy of the beta emission and the thinness of the particular source employed make precise detail of the active element less critical. The ^{106}Ru/Rh model hot particle source used in the present work (designed as ERU1) was constructed by inserting a commercially available electrodeposited ^{106}Ru/Rh disc source in a stainless steel needle capsulation (fig. 1 (a)) into a standard aluminum mount (fig. 1 (b)). This construction was simulated exactly according to the chemical composition and source geometry.

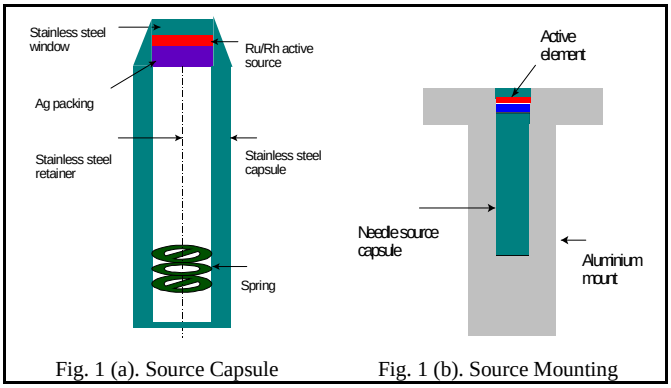

Fig. 1 (a). Source Capsule Fig. 1 (b). Source Mounting

Measurements of Dose Distribution

Three different techniques, Imaging Photon Detector IPD, RadioChromic Dye Film RDF and Extrapolation Chamber ECH were used for measuring radiation dose.

For IPD, thin Clear Fused Quartz CFQ (200 µm) dosemeters were used in order to measure the spatial and depth dose distributions around a ^{106}Ru/Rh model hot particle. Groups of stacks of dosemeters were used for direct irradiation inside a perspex jig using the source with its mounting. The dosemeters were left for six hours after irradiation to allow for the decay of low temperature peaks. The measurements on the IPD were carried out in the temperature range 50-150℃. The experiment was repeated with different exposure time for

different irradiated stacks in order for deep layer dose estimation. The doses were measured by CFQ over the area indicated at depths 23.8, 67.8, 111.8, 155.8, 199.8, 243.8, 287.8, 331.8, 375.8, 419.8 and 463.8 mg cm^{-2}.

For RDF technique, the GafChromic™ type HD810 dosimetry media used in this study have a thin (6.5 µm) radiation sensitive layer coated on a 100 µm thick polyester base. The exposed films were read out using a scanning micro- densitometer and calibrated against a standard ion chamber using a ^{60}Co teletherapy source. The scanning micro-densitometer principally used for read out in this work was a Joyce Loebl MDM6 mechanical object-plane scanner capable of measuring at high resolution with good dimensional and densitometric accuracy. The dose distributions averaged over areas at depths 1.3, 16.7, 31.6, 46.5, 61.4, 144.3, 212.3, 498.3 and 641.3 mg cm^{-2} were done.

For ECH technique, the chamber is a parallel plate ionisation chamber in which the separation between the electrodes can be progressively reduced to more closely approximate an ideal Bragg- Gray cavity The terminal slope $(dI/dx)_{x=>0}$ of the ionisation current (I) versus chamber electrode separation (x) curve is directly related to the absorbed dose in the cavity. In practice, for the Loevinger type chamber used in the present work, the extrapolation of the measurements is made using a set of simple functional forms of increasing nonlinearity. In the measurements on the $^{106}Ru/Rh$ source observation of the distribution of intercept values obtained by applying all the models to all the measurements with a particular electrode/window combination allowed inappropriate models to be more confidently rejected and a best estimate to be calculated from the remainder. To minimise the divergence between extrapolation models it is essential that the final chamber position is as close as possible to the minimum operable separation at which instability begins to occur. Furthermore, the onset of instability at small electrode separations was also monitored and identified.

Calculations of Dose Distributions

Spatial and depth dose distributions around a $^{106}Ru/Rh$ model hot particle were calculated using the EGS4(dosrz) with default PRESTA-I and EGSnrcMP with default inputs [19]. The experimental setup for RDF, IPD and ECH was simulated and the dose was scored in all media for energy conservation purposes. For the stopping power data the ICRU-37 density corrections were used in the PEGS4 data [20-21]. The source spectrum was used as energy bins of 25 KeV energy width for both ^{106}Ru and ^{106}Rh beta particles. Two identical codes were run separately for the two radio-nuclides. Other codes were run for three different gamma lines (0.512, 0.622 and 1.05 MeV) and the results were normalised according to their intensity. The particles were followed, during the simulation, until a cut-off energy AE of 512 keV (1 KeV kinetic energy) for electrons and a cut-off energy AP of 1 KeV for photons. The doses were calculated as gray per history and corrected as gray per hour using the source activity at the time of irradiation.

Result and discussion

The materials used in these simulations are polyester, aluminum, stainless steel, ruthenium, air, clear fused quartz and silver. The data for these materials were created by a standalone program PEGS4 code. The data were investigated using EXAMIN code by calculating the collision and radiative stopping power for electrons, the photon mean free path and the relative components of photon cross sections. The ICRU density corrections were used. For example fig. 2 shows the comparisons for both collision and radiative stopping power of electrons for aluminum. The created data, on one hand, were compared with the published one to make sure that the data creation by PEGS4 can be reliable. On the other hand, beta spectrum of ^{106}Rh hot particle with the cylindrical shapes are calculated to check the EGSnrc code capability to simulate the published point source spectrum of ^{106}Rh hot particle.

Non-uniform spatial Dose distributions measured using RDF, CFQ and ECH were simulated using both EGS4 and EGSnrcMP Monte Carlo Codes at the same depths and areas.

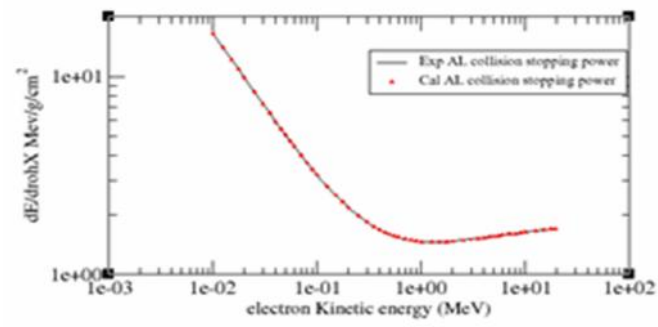

Fig. 2 (a). Calculated (PEG4) and published (ICRU) collision stopping power for aluminum.

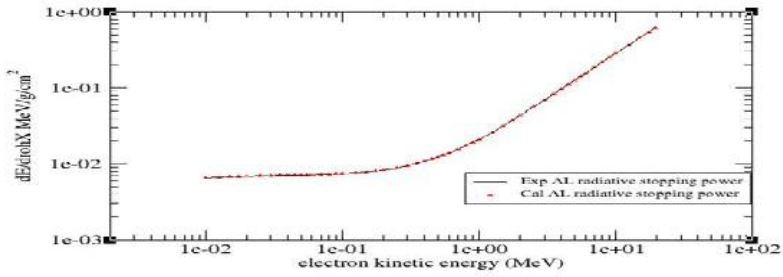

Fig. 2 (b). Calculated (PEG4) and published (ICRU) radiative stopping power for aluminum.

Since the radial dose distributions are investigated using small area dosemeters compared to the whole range of ^{106}Ru/Rh beta particles, the dose curves are represented as dose rate vs depth as appropriate. Figures (3.a) and (3.b) give the calculated beta/gamma dose ratio and dose distributions, respectively for CFQ with depths at areas 0.025, 0.071, 0.283, 0.785, 1.767, 3.142 and 7.069 cm^2.

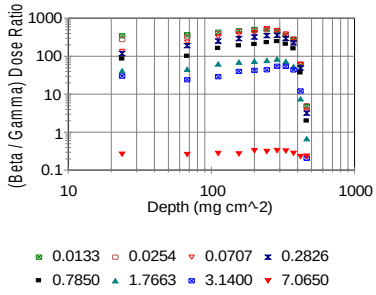

Fig. 3 (a). Calculated Beta / Gamma Dose Ratios using EGSnrcMP for CFQ dosemeters

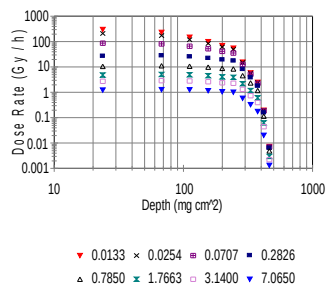

Fig. 3 (b). Calculated Dose Distributions using EGSnrcMP for CFQ dosemeters

Figures (4.a) and (4.b) give the calculated beta/gamma dose ratio and dose distributions, respectively for ECH with depths at areas 0.025, 0.071, 0.283, 0.785, 1.767, 3.142 and 7.069 cm^2. The figures show the build-up and fall-down regions.

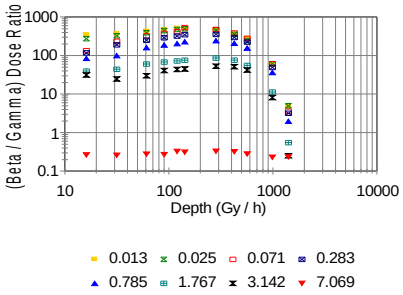

Fig. 4 (a). Calculated Beta / Gamma Dose Ratios using EGSnrcMP for ECH technique

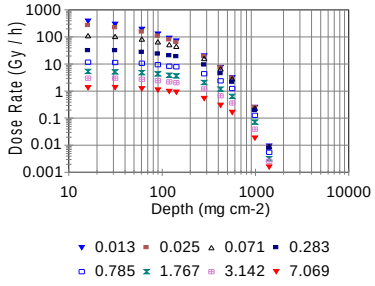

Fig. 4 (b). Calculated Dose Distributions using EGSnrcMP for ECH technique

Ratios of the dose rates predicted by both EGS4 and EGSnrcMP to those measured using ECH, RDF and IPD(CFQ) for the ^{106}Ru/Rh model hot particle have been evaluated. Measurements are grouped according to averaging area and depth. Measurements where anomalous intercepts were identified have not been included as they presently cannot be considered to be of adequate reliability.

The general agreement between the measurements and code predictions for EGS4 is reasonably good as shown in table 1. Overall ratios of 1.31 ± 0.42, 1.02 ± 0.21 and 1.12 ± 0.08 for ECH, RDF and IPD(CFQ), respectively show some evidence of a possible systematic tendency for the EGS4 code to overestimate the measurements for the higher

energy sources at small averaging areas. In the area range from 0.5 to 5.0 cm^2; of particular importance in respect of current radiological protection criteria, the agreement is somewhat improved, compared to ^{60}Co and ^{170}Tm model hot particles, with overall ratios of 1.03 ± 0.03 for IPD(CFQ) compared to 0.87±0.02 and 0.85±0.04 for ECH and RDF, respectively.

TABLE 1:COMPARISONS OF SPATIAL DOSE BETWEEN EGS4 AND MEASUREMENTS

Area (cm^2)	Depth ($mg\ cm^{-2}$)	EGS4 /ECH	EGS4 /RDF	EGS4 /IPD	Average	Standard Deviation
	00-10	1.50	1.30	1.24	1.35	0.14
	10-30	1.91	1.24	1.23	1.46	0.39
	30-50	1.90	1.24	1.21	1.45	0.39
0.005-0.05	50-100	1.90	1.34	1.15	1.46	0.39
	00-10	1.16	0.89	1.20	1.08	0.17
	10-30	1.17	0.92	1.13	1.07	0.13
	30-50	1.25	0.81	1.09	1.05	0.22
0.050-0.50	50-100	1.44	1.08	1.11	1.21	0.20
	00-10	0.86	0.81	1.01	0.89	0.10
	10-30	0.86	0.83	1.00	0.90	0.09
	30-50	0.88	0.88	1.06	0.94	0.10
0.500-5.00	50-100	0.90	0.91	1.07	0.96	0.10
Average		1.31	1.02	1.13	1.15	0.15
Standard Deviation		0.42	0.21	0.08	0.24	0.17

For EGSnrcMP, the general agreement between the measurements and code predictions is found better than that for EGS4 as shown in table 2.

TABLE 2: COMPARISONS OF SPATIAL DOSE BETWEEN EGSnrcMP AND MEASUREMENTS

Area (cm^2)	Depth ($mg\ cm^{-2}$)	EGSnrc /ECH	EGSnrc /RDF	EGSnrc /IPD	Average	Standard Deviation
	00-10	1.22	1.15	1.30	1.22	0.08
	10-30	1.34	1.17	1.20	1.24	0.09
	30-50	1.30	1.18	1.15	1.21	0.08
0.005-0.05	50-100	1.30	1.20	1.10	1.20	0.10
	00-10	1.10	1.10	1.10	1.10	0.00
	10-30	1.10	0.97	1.10	1.06	0.08
	30-50	1.17	0.94	1.05	1.05	0.12
0.050-0.50	50-100	1.22	0.96	1.20	1.13	0.14
	00-10	0.98	0.95	1.01	0.98	0.03
	10-30	0.94	0.90	1.04	0.96	0.07
	30-50	0.91	0.90	1.10	0.97	0.11
0.500-5.00	50-100	0.93	0.95	1.10	0.99	0.09
Average		1.13	1.03	1.12	1.09	0.05
Standard Deviation		0.16	0.12	0.08	0.12	0.04

Overall ratios of 1.13 ± 0.16, 1.03 ± 0.12 and 1.12 ± 0.08 for ECH, RDF and IPD(CFQ), respectively still show some evidence of a possible systematic tendency for the EGSnrcMP code to overestimate the measurements for the higher energy sources at small averaging areas and underestimate at big areas. But this over and under estimate decreased by more than 50% which means enhanced results for the whole simulation. In the area range from 0.5 to 5.0 cm^2; of particular importance in respect of current radiological protection criteria, the agreement is somewhat improved, compared to ^{60}Co and ^{170}Tm model hot particles, with overall ratios of 1.01 ± 0.03 for IPD(CFQ) compared to 0.98±0.02 and 0.95±0.04 for ECH and RDF, respectively.

In terms of overall agreement with the code predictions, RDF exhibits the best compared to other techniques with 1.08 ± 0.19 against EGS4. But in terms of consistent results for different areas and depths IPD(CFQ) measurements exhibit the best agreement with both EGS4 and EGSnrcMP code predictions. There is a tendency for underestimation by the ECH at small averaging areas with the $^{106}Ru/Rh$ model hot particle. It would therefore appear that, for $^{106}Ru/Rh$ model hot particle sources used in the inter-comparison, the general purpose EGS Monte Carlo codes are capable of providing dose estimates for the areas and depths of interest in radiological protection with an accuracy comparable with that attainable using available laboratory measurement techniques.

CONCLUSION

Hot particle hazards exist in the nuclear power industry, in the processing of radioactive ore, in medical, industrial and research applications of radioactive isotopes and around accelerators. The current work is an extension to a previous work for evaluating Monte Carlo code and different measurement techniques in measuring spatial dose distributions around high energy emitting $^{106}Ru/Rh$ model hot particle. For radiological protection purpose, the agreement between measurements and calculations is good. An overall revision of this work with that of ^{60}Co and ^{170}Tm is required. Furthermore, the effect of geometrical shape of hot particles directly put on the skin should be investigated to reflect the real situation of hot particles in the environment.

REFERENCES

[1] M. W. Charles, “The Hot Particle Problem.” Radiation Protection Dosimetry, (1991), 39: 39-47.
[2] Geesaman, D. P. (1968). “An Analysis of the Carcinogenetic Risk from an Insoluble Alpha Emitting Aerosol Deposited in Deep Respiratory Tissue.” Berkeley, University of California UCRL-50387.
[3] P. N. Dean, and W. H. Langham. “Tumorigenicity of Small Highly Radioactive Particles.” Health Phys. (1969) 16: 79-84.
[4] C. A. Sondhaus. “Some Toughts on Victor P Bond and His Work.” Health Phys. , (1996)70: 780.
[5] D. W. James,. “Problem Assessment of Discrete Radioactive Particles.” Elect. Power Res. Inst. (1988) EPRI-Report NP-5969.

[6] V. C. Rogers, and J. N. Vance. “Below Regulatory Concern Ownwer’s Group: Assessment of Discrete Radioactive Particle Dose.” Elect. Power Res. Inst. (1989) EPRI-Report NP-5678.
[7] J. J. Kelly, and S. Gustafson. “Industry Experience with Discrete Radioactive Particles.” Elect. Power Res. Inst. (1994) EPRI-Report TR-104125.
[8] I. G Mandjukov, B. V. Mandjukova, A. Alexiev and T. Andreev. “High Activity ot Particles in Kozloduy Nuclear Power Plant-Status of the Investigations.” Radiat. Prot. Dosim. (1994) 54: 133-138.
[9] ICRP. “1990 Recommendations of the International Commission on Radiological Protection. ICRP Publication 60.” Annals of the ICRP (1990) 21(1-3).
[10] ICRP. “The biological basis for skin dose limitation. ICRP publication 59.” Annals of the ICRP (1991) 22(2).
[11] I. E. Othman, Development of methods for evaluating radiation doses from hot particles. Birmingham, Cell Pysics Group, Shool of Physics and Astronomy Birmingham University (1998): MTR-98.
[12] I. E. Othman, and M. W. Charles. “Thermoluminescence properties of novel thin clear fused quartz (CFQ) dosemeters.” Radiation Protection Dosimetry (1998) 84(1-4): 193-199.
[13] I. E. Othman, and M. W. Charles. Hot particle dose measurements and calculations using the Monte Carlo code EGS4 and a thermoluminescence imaging photon detector. 11th International Congress of Radiation Research, Dublin, Ireland(1999).
[14] I. E. Othman, M. W. Charles and P. J. Darley. Beta dose measurements and calculations around 170Tm model hot particle using the Monte Carlo code EGS4 and Thermoluminescence Imaging Photon Detector. Intern. Conf. on Advanc. Monte Carlo for Radiat. Phys., Part. Trans. Simulat. and Apps., Lisbon, Portugal (2000).
[15] P. J. Darley, M. W. Charles, I. E. Othman, A. S. Al-Aydarous and A. J. Mill. “Origins and dosimetry of ‘hot particles’ from nuclear plant operation.” Radiat. Prot. Dosim. (2000) 92(1-3): 131-137.
[16] P. J. Darley, I. E. Othman and A. S. Al-Aydarous. Dosimetry intercomparisons for 106Ru Hot Particles. Birmingham, Cell Pysics Group, Shool of Physics and Astronomy Birmingham University: (2000) PR HPD/00/01.
[17] P. J.Darley, I. E. Othman and A. S. Al-Aydarous. Hot Particle Radiation Dosimetry: Development and validation of measurement and calculation techniques. Birminham, Cell Pysics Group, Shool of Physics and Astronomy Birmingham University: (2000) FR HPD/00.
[18] P. J.Darley, Villarreal-Barajas and I. E. Othman. Hot Particle Radiation Dosimetry: Development and validation of measurement and calculation techniques for hot particles. Birminham, Cell Pysics Group, Shool of Physics and Astronomy Birmingham University (1999): AR HPD/99.
[19] NRCC Report PIRS-701 The EGSnrc Code System:Monte Carlo Simulation of Electron and Photon Transport, March 31, 2013.
[20] ICRU. “ICRU Report 37, Stopping Powers for Electrons and Positrons.” (1984).
[21] ICRU. “Stopping Power for Electrons and Positrons.” (1984).

Redundancy of conventional cytogenetics with the development of molecular cytogenetic techniques

Teka A Ibrahim [1]., Elgubbi S Huda[2], Elzghied I Adam[3].

1, 3 Libyan foundation for research / science and technology
2 Faculty of science –Plant Department- Misurata

Abstract— The study of chromosome by microscopy started to become a reality when Tjio and Levan discovered the correct number of human chromosomes is 46. The development of banding techniques permitted the unique identification of each chromosome. Two most important early technical developments are the introduction of phyto-hemagglutinin, which allowed chromosome preparations to be made within 2 to 3 days from peripheral blood samples, and the use of colchicine to accumulate cells in metaphase in order to enhance observation after short-term culture. Conventional banding techniques like Q-banding, solid staining, G-banding, R-banding, C-banding, DAPI banding, Ag-NOR banding, replication banding, sister chromatid exchanges; are immensely useful in experimental situations, However, with the discovery that isotopically labeled DNA probes could be annealed to the complementary DNA sequences, the era of in-situ hybridization emerged and flourished after a nonisotopic method, fluorescence in situ hybridization (FISH), being developed.

INTRODUCTION

Cytogenetics is the study of chromosome by microscopy [1]. It started to become a reality when Tjio and Levan discovered the correct number of human chromosomes is 46. The development of banding techniques permitted the unique identification of each chromosome. Two most important early technical developments are the intrduction of phytohemagglutinin, which allowed chromosome preparations to be made within 2 to 3 days from peripheral blood samples [2], and the use of colchicine to accumulate cells in metaphase in order to enhance observation after short-term culture. Conventional banding techniques like Q-banding, solid staining, G-banding, R-banding, C-banding, DAPI banding, Ag-NOR banding, replication banding, sister chromatid exchanges…etc are immensely useful in experimental situations and in the precise characterization of chromosomal aberrations. High resolution banding of extended chromosomes in cells arrested in prophase or prometaphase was devised in 1970s [3,4]. However, with the discovery that isotopically labeled DNA probes could be annealed to the complementary DNA sequences, the era of in-situ hybridization emerged 1970s [5] and flourished after a nonisotopic method, fluorescence in situ hybridization (FISH), being developed Landegent et al.[6].

On the other hand, the development of molecular biology especially the discovery of PCR [7], the advent of flow cytometry [8] and the progress of FISH-based techniques together made the birth of a new branch of cytogenetics: molecular cytogenetics. It is extensively used as a powerful tool in genetic research and pratice. Nowadays, cytogenetic analysis (including molecular cytogenetics) is widely used in clinical genetics, cancer genetics, genomic research, evolutional genetics and many other biomedical fields. Will conventional cytogenetics soon be redundant with the advent and development of

molecular cytogenetics in a clinical diagnostic setting? Or most molecular cytogenetic tools remain applicable only in a research setting? As many authors said, clinical cytogenetic analysis demands speed, resolution and accuracy [9] and conventional banding is comparatively simple to achieve and is inexpensive [1]. While the reasons of the above comments made by these respected scholars need detailed examination and discussion. To answer this question, the advantages and the limitations of each cytogenetic technique (including the conventional banding) should be discussed in order to help clarify the different roles of these techniques in the service and research of genetics.

Indications For Cytogenetic Analysis [1]

1. Confirmation or exclusion of the diagnosis for known chromosomal syndromes
2. Unexplained psychomotor retardation with or without dysmorphic features
3. Abnormalities of sexual differentiation and development
4. Infertility
5. Monogenic disorders associated with mental retardation and or dysmorphic features
6. Recurrent miscarriage or stillbirth
7. Pregnancies shown to be at risk of aneuploidy from the results of maternal serum screening or fetal ultrasound scanning
8. Neoplastic conditions, particularly hematologic malignancies, for which the identification of specific chromosomal aberrations may be valuable in diagnosis and management

Chromosomal Abnormalities Detected By Cytogenetic Analysis

Aneuploidy (including trisomy, monosomy), hyperploidy disorders, reciprocal translocation, Robertsonian (centric fusion) translocation, insertional translocation, deletions/duplications, paracentric/pericentric inversions, isochromosomes, ring chromosomes and marker chromosomes are the common types of chromosomal abnormalities we met in the routine cytogenetic analysis. Detailed description of these abnormalities here goes a bit far from the theme of the essay question.

Methods In Cytogenetic Analysis

Conventional Banding

Conventional banding is capable of identifying every human chromosome and the origin of most larger chromosomal structural rearrangements [1]. Its ability to detect smaller chromosomal segments, e.g. segments less than 4Mb, is poor and thus should be used in conjunction with in situ methods in some cases. However, conventional banding techniques have made possible the rapid identification of an enormous range of karyotypic abnormalities. Here I give a brief review of these banding techniques and their

main applications. Figure 1 show the preparation of two most common tissue samples sent for karyotyping: the venous blood and the amniocytes retrieved from amniocentesis.

Solid staining

The chromosomes are exposed to a Giemsa or similar stain that has an affinity for DNA, yielding a uniformly dark appearance to the chromatids. This technique now is of limited use while still has applications in the investigation of fragile sites, scoring radiation damage, study of chromosomal breakage syndromes and evaluation of marker chromosomes.

Q-banding, G-banding, R-banding and High-Resolution banding

Caspersson et al. [1970, ref 10] firstly used quinacrine mustard to stain the chromosomes and examined with fluorescent microscope to discover the Q-banding. However, the Q-banding was soon replaced by other banding techniques because the fluorescence fades quickly. Conversely, G-banding is the benchmark of cytogenetic analysis and it's permanent. The G-dark bands are relatively AT-rich and roughly correspond to Q-bright and R-weak bands (see below, R-banding). Some 300 G-bands are readily distinguishable in the haploid genome at metaphase and 850-1250 bands at prometaphase and prophase [ISCN, 1995, ref 11]. For high resolution G- or R-banding, dividing cells are blocked in the S phase with methotrexate. When the block is released with thymidine-rich medium, the cell cycles of most cells are synchronized in the desired stage to be studied. Reverse banding, namely R-banding, was discovered by Dutrillaux and Lejune in 1971 [12]. Its banding pattern is approximately the reverse of the G- or Q-banding patterns. The main advantage of R-banding over G-banding is that the telomeres can be stained strongly instead of the light stain in G-banding. Each chromosome therefore can be identified through the banding techniques and the idiogram of human chromosomes is sketched. Figure 3 shows the karyotype and idiogram of normal human chromosomes.

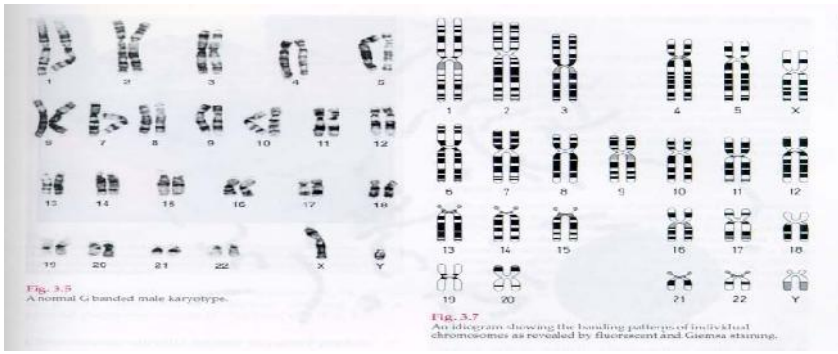

Figure 1. Karyotype and idiogram of normal human chromosomes

C-banding, DAPI banding and Ag-NOR banding

The C-banding was discovered by accident when chromosome spreads were heated to denature the DNA and the Giemsa staining of the chromosomes was greatly reduced except in the centromeric regions of most chromosomes and the distal part of Yq. A number of ways can be used to produce C-banding. The most common method is to treat chromosomes briefly with acid then with an alkali prior to Giemsa staining [12]. Heterochromatin can be stained and prominent C-bands are found on chromosome 1, 9, 16, and distal Yq. The heteromorphisms over the satellites of acrocentric chromosomes showed great variability in the population and was used to be markers in gene mapping, paternity testing, distinguishing monozygotic from dizygotic twins or the parent of origin of trisomy and triploidy. However, most these applications have been replaced by more precise molecular cytogenetic methods. DAPI (4,6-diamidino-2-phenylindole) banding and DAPI-DA (distamycin A) counterstaining also result in brightly fluorescing centromeric regions of chromosome 1, 9, 16 and distal Yq. In addition, DAPI-DA counterstaining especially highlighted a region on the proximal short arm of chromosome 15, which is the origin of a clinically important subgroup of marker chromosomes with a high risk of abnormal phenotype [1]. Ag-NOR staining can stain the satellite stalk regions of the acrocentric chromosomes which contain r-RNA coding sequences associated with the NOR (nucleolus organizer regions) of interphase nuclei. It is particularly useful in identification of acrocentric-derived chromosomes.

Replication banding and sister chromatid exchange

Replication banding uses BrdU to study timing of DNA replication. The reverse bands replicate during the first half of the S period and the Q- or G- bands replicate during the second half of S [12]. It is often used in the identification of late-replicating X chromosome in the studying structurally abnormal X chromosomes [1]. Differential staining of two sister chromatids in the C-band regions has been observed after BrdU being incorporated into DNA during replication [12] and may be used to demonstrate the sister chromatid exchange [13]. In contrast to X-ray exposure, which induces double- stranded breakage in a linear dose-dependent fashion but without increase in sister chromatid exchange (SCE), chemical mutagens induce SCE and thus can be detected [13].

Flow Karyotyping

Flow cytometry is capable of measuring and recording the DNA content of individual chromosomes as they pass in a fluid stream through the laser beam of a fluorescence-activated cell sorter (FACS). Monovariate histogram was initially used but only 15 peaks out of 24 chromosomes were seen. Bivariate system using Hoechst 33258 (affinity to AT-rich DNA) and chromomycin A3 (affinity to GC-rich DNA) can make a better separation in

the histogram except between chromosomes 9-12. The advantages of flow cytometry are: (1) all chromosomes are taken into account without the need to eliminate overlapping or poorly spread chromosomes (2) isolation of pure chromosomal fractions which can be used in the generation of probes for chromosome painting and in the construction of chromosome-specific gene libraries. However, the long time spent in this procedure remains a major limitation and thus flow cytometry remains mostly a research tool or used in preparation of chromosome-specific libraries (see later discussions) [15].

FISH (Fluorescence In Situ Hybridisation)

Principles

DNA is an elegant molecule with the fascinating property that complementarity (A to T and C to G, via hydrogen bond) of the nucleotide bases in its two anti-parallel strands. Denaturing the two strands can be achieved by heating (or other methods). Reannealing can be achieved by reducing the temperature under the suitable salt conditions. If a high concentration of labeled probe DNA is used, hybridization to complementary nucleic acid sequence in the target sequence can be achieved. Detection of the labeled DNA will identify the site of hybridization and thus the actual position of the target sequence.(See Figure 4). These properties make it possible to detect specific DNA sequences on a nitrocellulose filter (molecular hybridisation) or in cytological preparations (in situ hybridisation). Radioisotopes like tritium (^{3}H) or radioactive iodine (^{125}I) were used to label the probe and detected by autoradiography. However, the scatter of radioactive disintegrations and the high background noise made it poor in resolution, harzadous and time-consuming [1]. The interspersed repetitive DNA sequences resulted in the non-specific hybridization and thus produced a high background noise. However, the introduction of CISSH (Chromosomal In Situ Suppression Hybridization), using preannealing genomic DNA or Cot 1 DNA to the probes before being hybridized, had solved the problem and made nonradioactive (enzyme or fluorescence) labeling techniques replace autoradiography because of their greater speed, resolution and reliability [16].

FISH probes

The classification of eukaryotic (including human) DNA sequences helps us to understand the relationship and content of the probes and the target sequences that probes aim. table 1.

Table 1. Classification of Eukaryotic DNA

Protein-coding genes
Solitary genes
Duplicated and diverged genes (functional gene families and nonfunctional pseudogenes)
Tandemly repeated genes encoding rRNA, 5S rRNA,
tRNA, and histones
Repetitious DNA
Simple-sequence DNA
Moderately repeated DNA (mobile DNA elements)
Transposons
Viral retrotransposons
Long interspersed elements (LINES; nonviral
retrotransposons; The most common is L1 LINE family, 600000 copies in human DNA and accounts for 15% genome)
Short interspersed elements (SINES; nonviral
retrotransposons; The most abundant is Alu sequence, 1 million copies in human DNA and accounts for 10% genome)
Unclassified spacer DNA

FISH probes are generated by plasmid (10kbp; ref 1), phage (25kbp; ref 1), cosmid (35k-55kbp; ref 16), BAC (150-250kb; ref 18) and YAC (300k-1500kbp; ref 19). The types of probes are:

(1) **α-satellite probe**: These probes are located at pericentromeric region of all human chromosomes and consist of conserved tandem repeat sequences. Each sequence is about 171bp. The copy number and the nucleotide sequence are unique to each chromosome (with some exception) and therefore are useful in detection of aneuploidy.

(2) **Single-copy probes**: Probes are generated from genomic DNA or cDNA in 200-500kbp to detect single copy genes and can be used to detect micro-deletion/duplication syndromes as well as disclosing suspected cryptic translocations.

(3) **Chromosome painting probes**: These are chromosome-specific probes covering the entire chromosomes and usually are generated by flow sorted chromosomes preparation and PCR-related techniques.

(4) **Translocation probes**: Translocation probes are also unique single copy probes derived from specific regions of the chromosomes involved in a translocation. Probes are labeled with two different fluorochromes (Fig5). This allows identify the translocation by the juxtaposition of two different color signals in a translocation event. These probes are particularly useful in the detection of cancer specific

translocations on interphase nuclei when metaphases are not available.

(5) **Subtelomeric/telomeric probes**: These probes are localized to the distal ends of chromosomes and are

used to screen subtelomeric/telomeric deletion/duplication. Idiopathic mental handicap is reported to associate with these abnormalities [20].

Applications of FISH

The resolution of FISH is 2-3 Mbp in metaphase, 50kbp in interphase and 1-5kb in fixed extended fiber [1]. FISH is fast, can be used in interphase or nondividing cells, doesn't need isolation of nucleic acids prior to probing [9], can localize the target sequence of interest in the nucleus and is applicable to heterogenous cell populations. FISH and FISH-based technologies make an astonishing list of powerful tools used in molecular cytogenetics, though the majority of them remain only useful in a research setting. I will give a brief review of these technologies. Practically, FISH is used in Glasgow to provide (1) Examination of metaphase chromosomes for a variety of microdeletion syndromes (2) Subtelomeric screening by multiprobe device (3) Interphase FISH for chromosome copy number assessment (4) Detection of clinically significant rearrangements in neoplastic samples on a variety of clinical material and cultured cells (5) Rapid diagnosis of aneuploidy involving chromosomes 13, 18, 21, X and Y in uncultured amniocytes [14].

Chromosome Painting by Multiplex FISH/Specrtal Karyotyping (SKY)

The development of digital image microscopy, cooled couple charge device camera (CCD) and appropriate computer software and hardware permit the complex image manipulation and interpretation of multiple simultaneous hybridizations. Colorizing FISH now becomes a very exciting field. 24 chromosome-painting probes produced in different colours by 5 fluorochromes in combination [21], or by 4 fluorochromes in different mixing ratio through ComBinatorial Ratio Labeling (COBRA) [22], were used to detect simultaneously every chromosome in a metaphase spread [16]. My discussion of multicolor FISH composes of three aspects: image processing, probe-preparation and limitations.

(1) Image processing: Multiplex FISH requires a series of image acquisitions with a change of optical filters, while SKY uses a Fourier spectroscopy and an interferometer to evaluate the fluorescence emission patterns in a single, longer image acquisition. The colours shown in the computer are pseudo-colours generated by computer software. The COBRA technoque now can achieve an M-FISH multiplicity of 48, 96 or even higher [22].

(2) Probe preparation: Nowadays many probes have been commercially available. However, the preparation and generation of probes being used in chromosome painting rely upon the assistance of PCR. Methods being used include IRE

(Interspersed Repetitive Element)-PCR like Alu- or L1-PCR, IRE-bubble PCR, linker-adaptor PCR and degenerate oligonucleotide primer (DOP) PCR to generate probes from chromosomes obtained from somatic cell hybrids (mouse-human cell hybrid, losing some human chromosomes after fusion) or enriched flow-sorted preparations. The basic working theory of those PCR-based techniques are using the interspersed repetitive sequences like L1, Alu to act as one or both primers of PCR and amplify the genome sequences flanked by IRE and IRE/adaptor/DOP and try to generated DNA fragments as evenly-distributed as possible to generate a chromosome-specific probe used for chromosome painting. Detailed discussion will make this essay too lengthy and can be found in the references given by Munroe [23], Vooijs [24], and He [25]. However, the nucleolar organizer region (NOR) of the acrocentric chromosomes share sequences with pericentromeric heterochromatin. Cross-hybridization to the acrocentric centromeres cannot be inhibited by CISSH and no chromosome-specific α-satellite sequences have been found in these acrocentric chromosomes. Therefore some authors using chromosomes from close-related primates (like great apes and gibbons) to generate probes for these human chromosomes. There is no human-type repetitive sequences existing in these primates and cross-hybridization is thus avoided [26].

(3) Limitation: Intra-chromosomal rearrangements such as most deletions, duplications, or inversions cannot be detected by chromosomal painting. But other structural abnormalities like translocation, marker chromosomes or numerical disorders like trisomies can be detected. The major advantage over conventional banding is the ability to tell the origin of marker chromosomes and complex structural rearrangements.

Chromosome Bar Code (CBC)

Lengauer and co-workers developed a novel chromosome coloured staining technique called “chromosomal bar code” in 1992. They used subregional DNA probes in different colours to generate colour bars in human chromosomes. Each chromosome, like conventional banding, has a specific pattern. They used “bar” to distinguish this pattern with “banding” achieved by conventional techniques. At that time they had 47 bars in the whole metaphase spread [27] and the most advanced group now has 110 bands per haploid chromosome set for the human karyotype [26]. This technique can detect the intrachromosomal rearrangements like duplication, deletion and inversion that M-FISH or SKY cannot afford. While its resolution power is still secondary to conventional banding. Its use remains in a research setting. It has been used in studying the evolutional, comparative genetics. The close relatives of human being, like chimpanzee and gibbons, share many common chromosomal segments to human and the evolutionary process seems to undergo some structural rearrangements. Using CBC can give abundant information in the homology and differences between species.

Reverse Painting

In identifying marker chromosomes and in studying cross-species comparative genomics, isolation of chromosomes or chromosomal segments in interest (e.g., marker chromosomes or gibbon chromosomes) to generate for probes to hybridize to normal human metaphase spread can help identify the origin and locations of chromosomal segments. This tool can be used in heterogenous materials while remains mostly in a research setting [28].

Primed In Situ Labeling (PRINS)

PRINS is a modification of FISH, which utilizes the principle of PCR on in situ preparations (on glass slide). It appears to be very sensitive and cost-effective compared to conventional FISH. The most attractive feature of PRINS is the short time required for the test (about 2-3 hours). Conventional FISH can sometimes cost up to $200 per test owing to the high cost of commercial probes. PRINS, on the other hand, cost only about $10 per testing. Oligonucleotides are very inexpensive and only a very small quantity of the primers is needed (quoted from VAMC, Memphis, Pathology website). A labeled oligonucleotide primer, which is adjacent to the region of interest, is annealed to the genome and replication in situ is initiated with Taq DNA polymerase. It gives good result in detection of moderate- to high-copy number sequences and in the low-copy sequences when the labeled product is at least 1kbp in length [29].

Comparative Genomic Hybridization (CGH) and High-Resolution CGH (HR-CGH)

CGH is an effective technique for characterizing the genetic constitution of cells from two different sources [9]. It is a molecular cytogenetic approach for genome-wide screening for differences in copy number of any DNA sequence between the test and reference individuals. It needs only a few nanogram of DNA as FISH probes [16]. Equal amount of differently labeled DNA from the test individual (green) and reference DNA (red) are cohybridized to normal metaphase spreads. The fluorescence ratios of green-to-red intensities are calculated along the chromosomes by a digital image analysis system. Duplication or overexpression gives an increased ratio while losses or deletion give a decreased ratio. CGH cannot detect balanced translocations because there is no net gain or loss while is particularly useful in tumour cytogenetics because it can overcome many limitations of karyotyping such as difficulty in primary tumour culture, low mitotic index in some tumours, poor chromosomal morphology and complex rearrangement. The resolution of CGH is 2Mbp in amplifications and 10Mbp in deletions [30] while a new modification of CGH technique called high resolution CGH can minimize the resolution of deletion detection down to 3Mbp [31], which is even better than that of conventional G-banding (4Mbp). Some American scientists used expressed RNA to act as the fluorescent probes instead of DNA and devised a novel technique of genome-wide scanning called Comparative Expressed Sequence Hybridization (CESH) and got satisfactory resolution

[32]. Since these techniques need only scanty DNA, they may have a promising future in preimplantation genetic diagnosis and have already been widely used in studying cancers (more than 1500 tumour DNA samples, according to ref 16).

Multiprobe

Submicroscopic rearrangement involving telomeres were reported to be associated with idiopathic mental retardation [20]. Most chromosome translocations involve chromosome ends and it is difficult to screen telomereric/subtelomereric subtle changes by conventional banding. It is now more acceptable that using telomeric screening by FISH in victims of idiopathic mental retardation after the developments of first- (NIH, Institute of Molecular Medicine Collaboration 1996, ref 33) and second- (Cytocell Ltd Multiprobe technique,ref 20) generation probe sets. The commercially available Cytocell Ltd Multiprobe® technique costs US$400 per test and using a multi-cell design over a single slide to screen the whole 24 chromosomes, including chromosome painting, centromeres and most telomeres, simultaneously.

Microarray

Hybridizations are performed on an array of DNA clones spotted on a slide. Using known gene sequences or EST (expression sequence tags) as probes to study the expression profiles of test tissue. We can use reverse transcriptase to make c-DNA from m-RNA to study the expression of thousands of genes simultaneously . Microarray is relatively inexpensive (as compared to other fancy tools), the capital cost for building both an arrayer and scanner is now less than US$60000 and the marginal cost per slide is about US$20, and fast (150 copies of an array of 12000 genes need only one day). However, its use in a clinical diagnostic setting is rare. Microarray technology needs sequence information and thus cannot screen unknown sequences. Despite that, it can be used to study the gene expression patterns in different tissues and different time scale and thus it is a powerful tool in post-genome biological research [34].

CONCLUSION

Cytogenetics has undergone significant advances since the development of banding techniques. However, fromthe above discussions it can be concluded that each molecular cytogenetic tool has its own strong and weak points. Conventional banding technique remains to be the golden standard to meet the requirements of a clinical diagnostic setting for its accuracy, speed, inexpensiveness and reliability. Many molecular cytogenetic tools haven’t reached a mature state to be provided clinically but do have an invaluable role in a research lab to focus upon certain specific studies especially suitable for them. Some tools may someday be mature enough to be provided routinely like the aneuploidy FISH at present. Unlike certain revolutionary change happened in the

informational technology like Windows replacing the DOS in the operating system, the role of molecular cytogenetics to the conventional cytogenetics is more like the rapid update of Microsoft Office to the basic operating scheme Windows. Of course, molecular cytogenetics (for example, SKY+CBC) someday may advance to be competitive enough and finally replaces the conventional cytogenetics in the daily clinical diagnostic setting with the progress of technology, but not now and even not in the near future.

REFERENCES

[1] 1. V. Malka et al., Nature Phys. **4**, 447 (2008).
[2] 2. E. Esarey et al., Nature **431**, 535 (2004).
[3] 4. C. G. R. Geddes et al., Nature **431**, 538 (2004).
[4] 5. J. Faure et al., Nature **431**, 541 (2004).
[5] 6. W. P. Leemans et al., Nature Phys. **2**, 696 (2006).
[6] 7. H.-P. Schlenvoigt et al., Nature Phys. **4**, 130 (2008).
[7] 8. M. Fuchs et al., Nature Phys. **5**, 826 (2009).
[8] 9. S. Cipiccia et al., Nature Phys. **7**, 867 (2011).
[9] 10. W. Lu et al., Phys. Rev. ST Accel. Beams **10**, 061301 (2007).11. S. M. Wiggins et al., Plasma Phys. Control. Fusion **52**,
[10] 124032 (2010).
[11] 12. C. E. Clayton et al., Phys. Rev. Lett. **105**, 105003 (2010).
[12] 13. C. McGuffey et al., Phys. Plasmas **16**, 113105 (2009).
[13] 14. H. Lu et al., Appl. Phys. Lett. **99**, 091502 (2011).
[14] 15. T. Katsouleas, Phys. Rev. A **33**, 2056 (1986).
[15] 16. P. Sprangle et al., Phys. Plasmas **9**, 2364 (2002).
[16] 17. W. Rittershofer et al., Phys. Plasmas **17**, 063104 (2010).
[17] 18. S. M. Wiggins et al., Rev. Sci. Instrum. **82**, 096104 (2011).
[18] 19. S. Abuazoum et al., Appl. Phys. Lett. **100**, 014106 (2012).
[19] 20. D. Kaganovich et al., Appl. Phys. Lett. **75**, 772 (1999).
[20] 21. E. Brunetti et al., Phys. Rev. Lett. **105**, 215007 (2010).
[21] 22. S. Abuazoum et al., Rev. Sci. Instrum. **82**, 063505 (2011).
[22] 23. D. J. Spence and S. M. Hooker, Phys. Rev. E **63**, 015401 (2001).
[23] 24. T. P. Rowlands-Rees et al., Phys. Rev. Lett. **100**, 105005 (2008).
[24] 25. S. Karsch et al., New J. Phys. **9**, 415 (2007).
[25] 26. A. J. Gonsalves et al., Phys. Rev. Lett. **98**, 025002 (2007).
[26] 27. D. G. Jang et al., Appl. Phys. Lett. **99**, 141502 (2011).
[27] 28. C. Rechatin et al., Phys. Rev. Lett. **102**, 164801 (2009).
[28] 29. T. Katsouleas et al., Part. Accel. **22**, 81 (1987).
[29] 30. S. van der Geer et al., in Computational Accelerator
[30] Physics 2002 Vol. 175 (Institute of Physics, Bristol, UK,
[31] 2005), p 101.
[32] . “Stopping Power for Electrons and Positrons.” (1984).

The Second Symposium on Theories and Applications of Basic and Biosciences 5 September 2015

Distributed Arithmetic Technique Analysis, Design and applications

Mohamed Al Mahdi Eshtawie

Computer Engineering Department

Libyan Academy Misurata
eshtawie@yahoo.com

Abstract- In modern data transmission systems, bits or group of bits, symbols, are typically transmitted in the form of individual pulses of energy. The basic properties of the rectangular pulse made it probably the most fundamental since it is clearly cannot cause interference during the sampling time of other pulses. The wide bandwidth occupied by the energy of the rectangular pulse made it unsuitable for modern transmission systems. For this reason, raised cosine filter is used to reduce the pulse bandwidth. The convolution equation that describes the relation between input samples and the filter coefficients is equivalent to a multiplication in the frequency domain. Therefore, as the number of input samples and filter coefficients goes high a large number of multiplications are needed to get the filter output. This will lead to a highly complex and costly design. Moreover, the overall speed of the system will be low. In digital signal processing the most-often encountered form of computation is a sum of products. Distributed arithmetic technique (DA) targets the sum of products computation that is found in many of the important DSP filtering and frequency transforming functions.

DA differs from conventional arithmetic only in the order in which it performs operations. In other words, DA is an algorithm that performs multiplication with a look-up table (DALUT) based scheme. Using of DALUT eliminates the need of multiplication operation and that will have a dramatic effect on the speed of the design. Hence sum of product equations are implemented serially without a need of performing multiplications. unfortunately, the DALUT which is the advantage of the DA causes a serious trouble due to its dramatic grow. This paper gives the analysis the basic principle of the distributed arithmetic its main advantages and major drawback. The design of DA systems is also illustrated. Different designs and their applications are also presented. Some of the hardware results are given for these different design approaches.

INTRODUCTION

Distributed arithmetic is an efficient technique for calculation of the inner product commonly applied in multiply and accumulate (MAC) function. MAC unit operation is common in Digital Signal Processing algorithms. In transmission systems where bits or group of bits or symbols, are typically transmitted in the form of individual pulses of energy. Distributed arithmetic technique (DA) targets the sum of products computation that is found in many of the important DSP filtering and frequency transforming functions [1]. The fundamental properties of pulses specify the basic requirement that does not cause any interference or energy loss while transmission. The basic properties of the rectangular pulse made it probably the most fundamental. Clearly, rectangular pulse can not cause interference during the sampling time of other pulses. It can be directly compared to

opening and closing a switch that resembles the concept of binary information. Therefore, it is easy to implement in a real-world systems. Unfortunately, the wide bandwidth occupied by the energy of this pulse, made its frequency response to be unsuitable for modern transmission systems. Hence raised cosine pulse, which is used in a wide variety of modern data transmission systems, is used to limit bandwidth i.e. decays quickly and provide zero crossing at the pulse sampling times.

By its definition, the pulse shape that is suitable for the required data transmission rate, the next step is to decide which digital filter to use. Filtering is one of the most useful signal processing operations [2]. There are two major types of digital filters, FIR and IIR. However, FIR filter has a certain advantages over the IIR i.e. linear phase, guaranteed stability, fewer finite precision errors, and efficient implementation [3].

The convolution equation that describes the relation between input samples and the filter coefficients is equivalent to a multiplication in the frequency domain. The convolution equation is simply represented by figure (1). This figure shows the basic flow of MAC unit that implemets the finite impulse response filters, for which distributed arithmetic is an efficient tool for implementation.

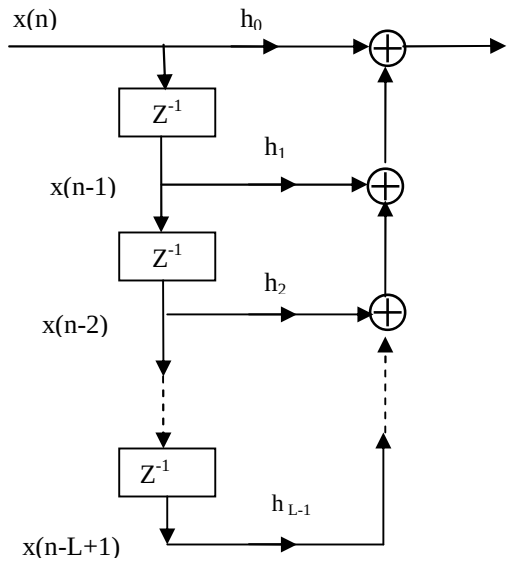

Figure 1 Signal Flow for FIR filters

Mathematically, this figure is represented essentially as a discrete convolution of the input signal with a set of coefficients. Equation 1 shows this relation.

$$y(n) = \sum_{k=0}^{L-1} h(k)x(n-k) \qquad (1)$$

Equation (1) clearly shows that its output is formed as a weighted sum of present and past samples of its input.

2. Distributed Arithmetic Architecture

Basically, DA is an algorithm that performs multiplication with a look-up table (LUT) based scheme as shown in Figure (2). Therefore; it is a computational operation that forms an inner (dot) product of a pair of vectors in a single direct step. The LUT contents are fetched when addressed through the values obtained from the shift register unit. The basic distributed arithmetic architecture is shown in Figure below.

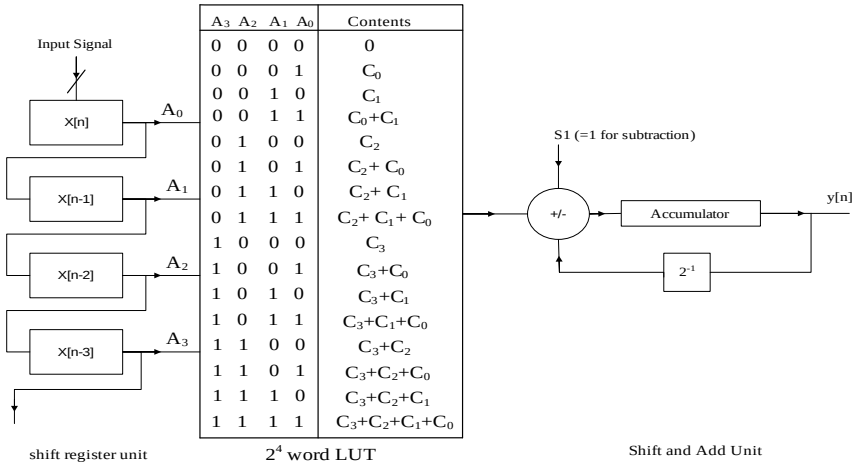

Figure (2) Basic Distributed Architecture

The input variable in the input-output relationship given in equation 1 that characterize the non recursive digital filters, can be represented in two's complement binary number so that,

$$x_k = -x_{k0} + \sum_{b=1}^{B-1} x_{kb}\, 2^{-b} \qquad (2)$$

x_{kb} , is a binary variable that can take values of 0 and 1. A sign bit of value -1 is represented by. Substituting (2) in (1) we get:

$$Y = \sum_{k=1}^{K} h[k] \cdot \left(-x_{k0} + \sum_{b=1}^{B-1} x_{b-1} \right) 2^{-b} \qquad (3)$$

$$= -\sum_{k=1}^{K} h[k]\, x_{k0} + \sum_{b=1}^{B-1} \left(\sum_{k=1}^{K} h[k]\, x_{kb} \right) 2^{-b} \qquad (4)$$

Equation (4) shows that the term $\sum_{k=1}^{K} h[k]x_{kb}$ has only 2^b possible values that can be precomputed and stored in the LUT. Each time the input variables are used to address the LUT contents, the result $\sum_{k=1}^{K} h[k]x_{kb}$ is dropped into an accumulator.

The problem with serial computation DA is not limited to fewer throughputs, but the size of LUT becomes very large when implementing high order filters. In other words, as the filter order increase by one, the size of the LUT is doubled. In the literature, this problem has been addressed using several techniques. In [4] and [5] multiple memory bank techniques is used to reduce the size of the LUT.

The following architecture (white 1989) shows that the signal x_1 is used as the add/subtract control signal for the buffer input. During the sign bit time, the add/subtract command must be inverted. Therefore, the signal x_1 is combined with T_s signal through EXOR gate in order to derive the proper add/subtract control signal. The value stored in the initial condition register is used to correct the value obtained from the ROM when addressed.

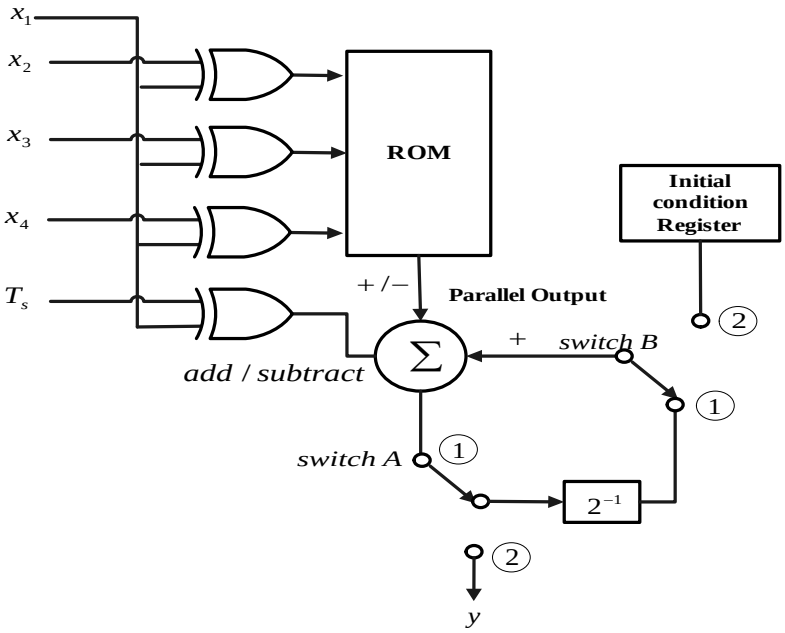

Figure (3) Adder/subtractor and reduced memory (White 1989)

(Choi et al 2000) proposed a design where the LUT size is further reduced by half. There, a control signal is used to distinguish between any two symmetrical locations in the LUT. In this case the LUT size is reduced to 2^{k-2} words. Figure 3 shows this architecture.

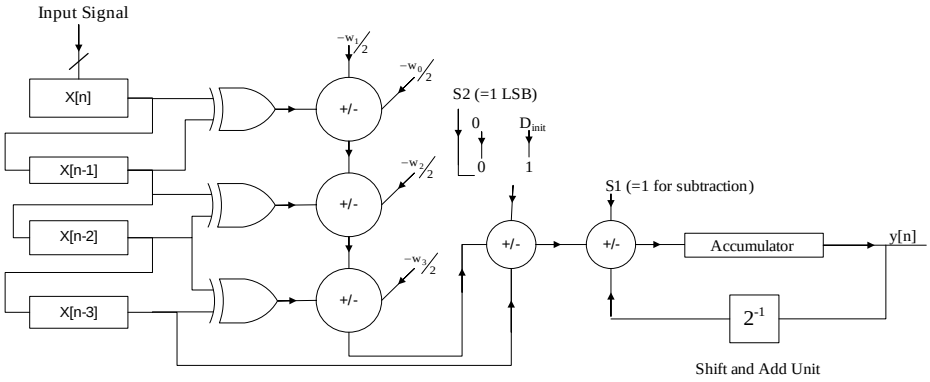

Figure 4 DA-OBC LUT-less Architecture

Equation (4) shows that the term has only 2^b possible values that can be precomputed and stored in the LUT. Therefore, as the number of input samples and filter coefficients goes high a large number of multiplications are needed to get the filter output. This will lead to a highly complex and costly design. Moreover, the overall speed of the system will be low.

Eshtawie (2006) has proposed an architecture that eliminates the need for the LUT and hence overcome the major drawback of this technique. The design basically applied digital carry lookahead adder and buffers that will forward the input if its value is 1. The following figure shows this architecture.

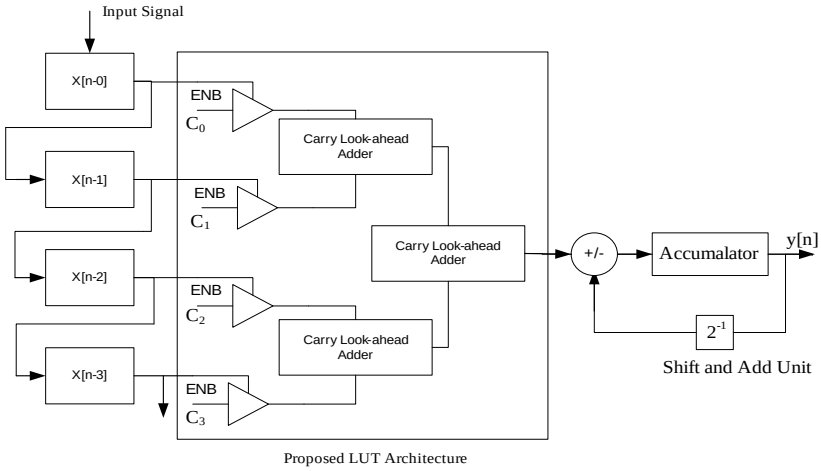

Figure (5) Online DALUT Architecture

The use of tri-state buffer and CLA as basic logic units in the proposed architecture imposes a remarkable improvement in speed and area-time efficiency parameters. Figiure 6 shows buffer if 1 (bufif1) primitive with four outputs.

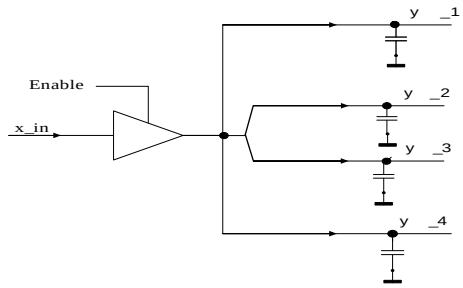

Figure (6) Buffer if 1 instantiation.

Here when the enable is asserted, the outputs are determined by the input x_in. Therefore, the enable signal which is any of the shift registers output bit, in Figure 4, is a primary condition whether to transfer its associated filter coefficient to the CLA in the next stage or not. This is the main concept of the DA technique presented in [6].

RESULTS AND DISCUSSION

Throughout the previous sections, the basic concept of the DA technique is discussed both in its hardware architecture and mathematical models that describe its internal operations and input processing. This section shows the results obtained for different designs when simulation is carried out using ModelSim 5.7g.

When LUT is eliminated, the architecture shown in Figure 5, then the computation time is highly effected by the type of adder implemented in the design. For this reason a comparison is done between different adders and the results are shown in figures below.

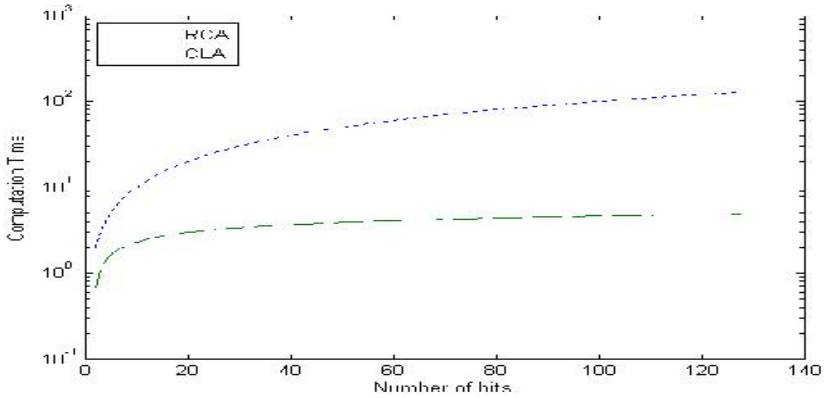

Figure (7) Computation Time for RCA and CLA

Figure 7 shows that the computation time for the CLA adder is much less than the RCA that has the worst computation time. on the other hand, the Area Time efficiency, for these two adders is given in Figure 8. In this figure it is clear that the performance of the architecture with the CLA is more closer to that of the RCA due to area consideration. The reason behind this comparison is that a new architecture for digital adder is proposed and that is called If-Then adder. This adder is implemented in the same manner done with the CLA. The results obtained from this architecture show the advantage of the proposed adder over the RCA and CLA in terms of area, and the advantage of speed over the RCA.

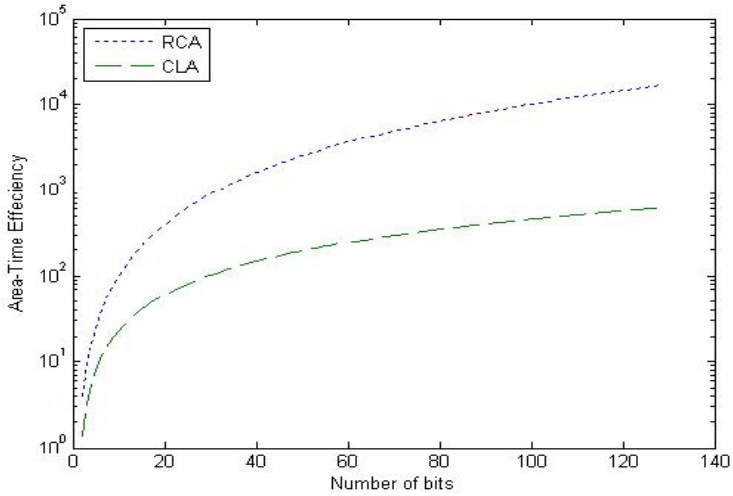

Figure (8) Area-Time Efficiency for RCA and CLA

The following Figures show the results obtained from synthesis and hardware simulation tools. For clarification, the results obtained for the adders in terms of maximum frequency is given first in Figure (9).

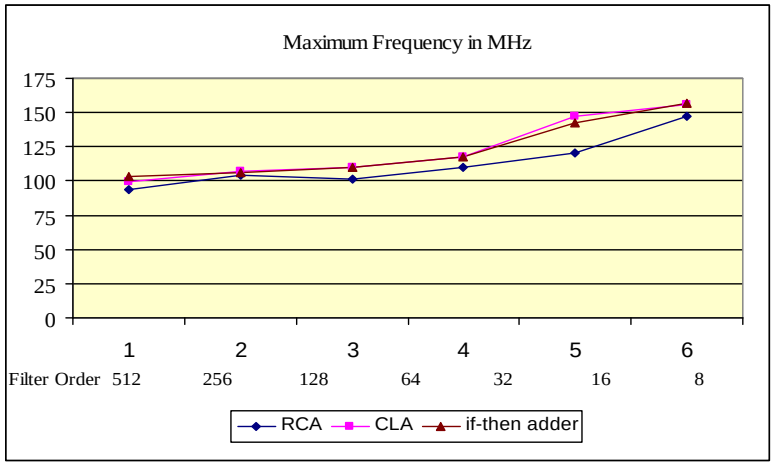

Figure ((9 Maximum frequency from Xilinx synthesis report

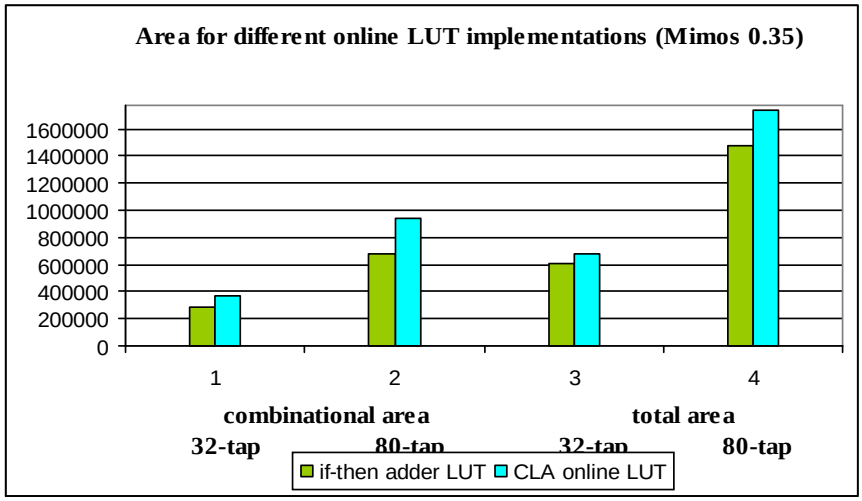

Figure)10) Total and combinational area for different LUT implementations

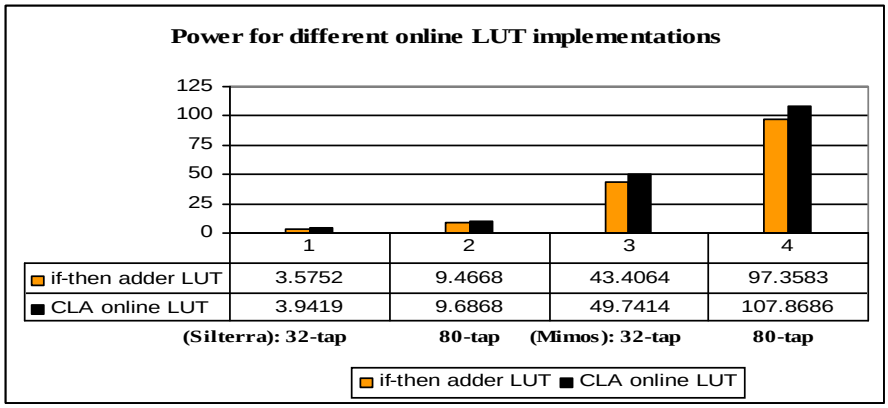

Figure (11) Total dynamic power for different LUT implementations

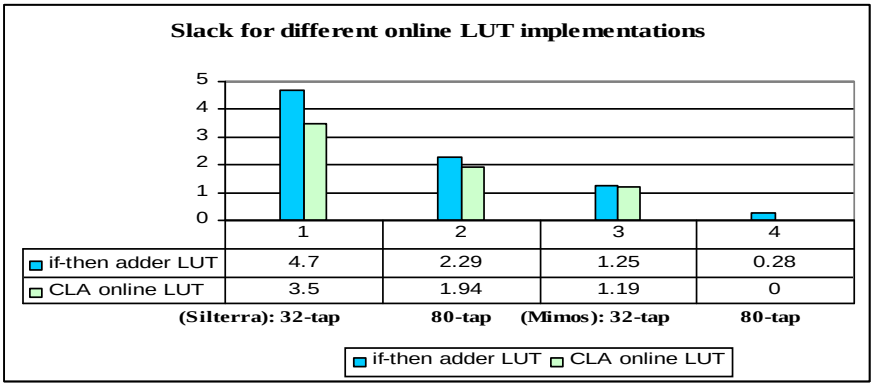

Figure ((12 Slack value for different LUT implementations

Figures above show different design approaches for the distributed arithmetic technique when designed and implemented without LUT as proposed in Figure 5. These results show that with this new design approach the number of inputs considered can be as large as required and that will influence the FIR filter order or in other words the number of taps applied in the design.

CONCLUSION

This paper presents the basic architecture and mathematical concept of the DA technique. Different design approaches for this techniques have been examined and tested in terms of hardware parameters i.e. the area, speed and power consumption. Different simulation packages have been applied to examine these designs parameters and the results obtained show the advantage of the proposed architecture and its various approaches. Xilinx Synthesis Technology (XST) and ModelSim 5.7g are among the packages applied to test different designs and the results obtained show the advantages of the proposed design over the basic and other architectures.

REFERENCES

1. Sungwook Yu and Earl E Swartzlander Jr. “DCT Implementation with distributed arithmetic”. IEEE transaction on Computers, Vol. 50 No. 9, September 2001.
2. A. Peled and B. Liu, “A new hardware Realization of Digital Filters,” IEEE Transactions. Acouustics, Speed and Signal Processing, vol. 22, pp. 456-462, 1974.
3. Stanley A. White, "Applications of distributed arithmetic to digital signal processing: A tutorial review," IEEE ASSP magazine July, 1989.
4. W.P. Burleson and L. L. Scharf, “A VLSI Design Methodology for Distributed Arithmetic,” J. VLSI Signal Processing, vol. 2 pp. 235-252,1991.
5. S. Wolter, A. Schubert, H. Matz, and R. Laur, “On the Comparison between Architectures for the Implementation of Distributed Arithmetic,” Proc. IEEE Int’l Symp. Citcuits and Systems, vol. 3 pp. 1829-1832,1993.
6. T. Salim, J. Devlin, and J Whittington, “FPGA Implementation of Digital Upconversion using Distributed Arithmetic FIR Filters,” ICFPT 2004, pp 335-338, 2004.
7. The Role of Distributed Arithmetic in FPGA Based Signal Processing, Xilinx Publications.

8. K. K. Parhi, “VLSI Digital Signal Processing Systems: Design and Implementation,” Published by John Wily and Sons 1999.
9. Heejong Yoo and David V. Anderson, "Hardware-Efficient Distributed Arithmetic Architecture for High Order Digital Filters," IEEE International Conference on Acoustics, Speech, and Signal Processing, pp. 125-128, Philadelphia, PA, USA, March 2005
10. Ruiph Chassaing, "DSP Application Using C and the TMS20C6x DSK", A Wiley-Interscience Publication, 2002.
11. Sen M. Kuo, Woon-Seng Can, "Digital Signal Processing Architecture, Implementations, and Applications", Prentice Hall 2005.
12. Radhika S. Grover, Weijia Shang and Qiang Li,"A Faster Distributed Arithmetic Architecture for FPGAs",FPGA'02, February 2002, California, USA.
13. N. K. Bose, Digital Filters: Theory and applications, 1985.
14. Kehtarnavaz N, Keramat M., "DSP System Design Using the TMS320C600" Upper Saddle River, NJ: Prentice Hall, 2001.
15. Michael D. Ciletti, "Advanced Digital Design with the VERILOG HDL, Prentice Hall 2003.
16. Mintzer, L. "FIR filters with the Xilinx FPGA" FPGA'92 ACM/SIGDA Workshop on FPGAs pp. 129-134.
17. Bernie New, "A distributed arithmetic approach to designing scalable DSP chips" EDN, August 1995.
18. Paul A. Lynn and Wolfgang Fuerst, "Introductory digital signal processing with computer applications", A Wiley-Interscience Publication, 2004.

The Second Symposium on Theories and Applications of Basic and Biosciences 5 September 2015

Genetic Basis of Colorectal Cancer

Mustafa Alsgier [1], Omar Alqawi [2]

[1] Mustafa Alsgier, Chemistry department, Faculty of Science, misurata university, Biotechnology research center, misurata, libya E-mail: Alsgier.mustafa@gmail.com
[2] Phd.Omar alqawi, Biotechnology research center, misurata, libya E-mail:oalqawi@hotmail.com

Abstract—Each year over 1.83 million people are diagnosed with colorectal cancer(CRC) worldwide , with an annual mortality of more than 694,000 making it the third most common cause of cancer mortality among men and women. The disease results from the progressive accumulation of genetic and epigenetic alterations that lead to the transformation of normal colonic epithelium to colon adenocarcinoma. The challenges are to understand the molecular basis of individual receptivity to colorectal cancer and to determine factors that initiate the development of the tumor, drive its progression, and determine its responsiveness or resistance to antitumor agents. Colorectal cancer is a heterogeneous disease, with four known major molecular aspects. The first is that the genetic and epigenetic alterations that cause colorectal cancer formation promote the cancer formation process because they provide a clonal growth advantage to the cells that acquire them. The second concept is that cancer arises via a multi-step progression at both the molecular and the morphologic level. The third is the loss of genomic stability can drive the development of colorectal cancer by facilitating the acquisition of multiple tumor-associated mutations. The fourth is that hereditary cancer syndromes frequently correspond to germ line forms of key genetic disorders whose somatic occurrences drive the emergence of sporadic colorectal cancers.in this paper we investigate the roles and relationships of these concepts and their interactions in colorectal cancer.

Keywords- Colorectal cancer, metastasis, tumour suppressor genes, oncogenes, KRAS, EGFR, Genetic instability.

INTRODUCTION

The colon is one of the fundamental parts of the digestive tract, as the largest and first of the segments of the large intestine, located between the small intestine and the rectum. Its principal functions are the absorption of water, minerals, and nutrients, and to serve as a storage area for the waste material that forms the feces. It consists of four sections: the ascending colon located on the right side; the transverse colon; the descending colon located on the left side, and the sigmoid colon or sigmoid. Together they constitute an irregular and thick organ because of the longitudinal disposition of muscular fibres, with a less developed submucosa, but a very evident mucosa as it is full of lymph nodes which confer its characteristic appearance. The mucosa, which is thicker than that of the small intestine, has multiple tubular invaginations called 'crypts of Lieberkühn', which are wide, deep, and numerous, along the surface of its epithelium, and in which the regeneration of the epithelium takes place [1]. Because of its biological nature, the colon has a high level of cellular regeneration and a physiological role in of physical, chemical, and biological nature, which increases the possibility of developing diverse pathologies, including cancer. Colorectal cancers are classified as well-differentiated, moderately well differentiated, or poorly differentiated on the degree of preservation of normal glandular architecture and cytologic features. Progressively more poor differentiation is presumably a histologic marker of further underlying genetic mutations, but the mutations associated with

poor differentiation are currently unknown. About 20% of cancers are poorly differentiated. They have a poor prognosis[2]. About 15% of colon cancers are classified as mucinous or colloid because of prominent intracellular accumulation of mucin. These cancers are more aggressive[3].

Colorectal cancer is recently staged according to the tumor–node–metastases (TNM) classification by mural depth of the primary tumor (T), by presence of local lymph node metastases (N), and by presence of distant metastases (M)[4]. This classification is particularly helpful in endosonographic staging of colorectal cancer[5]. In the TNM classification, invasive colon cancer is classified from stage I to IV. Stage I in the TNM classification corresponds to Dukes A or B1 lesions, stage II corresponds to a Dukes B2 lesion, stage III corresponds to a Dukes C lesion, and stage IV corresponds to a Dukes D lesion. Pathologic stage is highly correlated with cancer prognosis[6].

GENETICS AND EPIGENITICS ALTERATIONS IN CRC

Colorectal cancer results from the progressive accumulation of genetic and epigenetic alterations that lead to the transformation of normal colonic epithelium to colon adenocarcinoma. From the analysis of the molecular genesis of colorectal cancer, four central tenets concerning the pathogenesis of cancer have been established. The first is that the genetic and epigenetic alterations that underlie colon cancer formation promote the cancer formation process because they provide a clonal growth advantage to the cells that acquire them. The second tenet is that cancer emerges via a multi-step progression at both the molecular and the morphologic levels[7] The third is that loss of genomic stability is a key molecular step in cancer formation[8] The fourth is that hereditary cancer syndromes frequently correspond to germ line forms of key genetic defects whose somatic occurrences drive the emergence of sporadic colorectal cancers[9].

A. GENETIC ALTRATIONS

Colorectal cancer is believed caused by a cascade of genetic mutations leading to progressively disordered local DNA replication and accelerated colonocyte replication. the progressive accumulation of multiple genetic mutations results in the transition from normal mucosa to benign adenoma to severe dysplasia to frank carcinoma (Table 1). A progression from normal mucosa to adenoma to carcinoma was supported by the demonstration of accumulating mutations in genes of APC, K-RAS, P53 and DCC, all of which are thought to be of significance, but are not able successfully to account for all CRCs. Mutations of the mismatch repair genes are believed to account for about 15% of sporadic colorectal cancers[10]. APC mutation is believed to account for about 80% of sporadic colorectal cancers[10]. alterations in APC, which result in overactivation of the Wingless/Wnt signalling pathway, appear to initiate tumour formation in the colon. Subsequent alterations in other genes then play a role in tumour growth and the eventual acquisition of other malignant characteristics such as tissue invasiveness and the ability to metastasize.

APC

The Adenomatous polyposis coli (APC) gene encodes a protein that possesses multiple functional domains that mediate oligomerization as well as binding to a variety of intracellular proteins including ß-catenin, γ-catenin, glycogen synthase kinase (GSK)-3ß, axin, tubulin, EB1, and Hdlg [9]. The activation of the Wnt signaling pathway, is regarded

as the initiating event in colorectal cancer . Wnt signaling occurs when the oncoprotein β-catenin binds to nuclear partners (members of the T-cell factor–lymphocyte enhancer factor family) to create a transcription factor that regulates genes involved in cellular activation[11][12][13]. The β-catenin degradation complex controls levels of the β-catenin protein by proteolysis. A component of this complex, APC, not only degrades β-catenin but also inhibits its nuclear localization.

One of the central tumour promoting effects of these mutations results in overactivation of the Wingless/Wnt signaling pathway, with the subsequent expression of genes that favor cell growth. APC mutations disrupt the association of APC with ß-catenin, resulting in excessive amounts of ß-catenin and overactivation of the Wnt signaling pathway. Consequently, genes that promote tumour formation are transcribed. Truncating APC mutations prevent this process from happening and cause an increase in the amount of cytoplasmic ß-catenin, which can then translocate to the nucleus and interact with other transcription factors.

P53

The normal tumour suppressor gene p53 product arrests the cell cycle following DNA injury to permit either DNA repair if the damage is correctable, or apoptosis if the damage is too severe. The wild-type p53 protein product is up-regulated after *cell stress from radiation exposure, DNA* injury, or other noxious events to prevent new DNA synthesis and halt cell division. Loss of function can promote genomic instability as genetic errors are replicated without check, resulting in loss of heterozygosity. Mutation of the p53 gene is believed to be important in the transition from late adenoma to frank carcinoma. About 50% of lesions with high-grade dysplasia and about 75% of frank cancers exhibit loss of normal p53 function, usually from a missense point mutation of one allele and deletion of the other, wild-type, allele[14][15] .

In colorectal cancers, P53 mutations have not been observed in colon adenomas, but rather appear to be late events in the colon adenoma-carcinoma sequence that may mediate the transition from adenoma to carcinoma[16]. Furthermore, mutation of P53 coupled with loss of heterozygosity (LOH) of the wild-type allele was found to coincide with the appearance of carcinoma in an adenoma, thus providing further evidence of its role in the transition to malignancy [17][18]. The function of P53 to recognize DNA damage and induce cell cycle arrest and DNA repair or apoptosis has led to P53 being called the “guardian of the genome”[19].

DCC

The DCC (deleted in colon cancer) gene encodes for a neural cell adhesion molecule receptor and normally promotes apoptosis and suppresses tumors. Loss of the normal DCC gene is believed to be important in the transition from an intermediate to a late adenoma. Its role in this transition is supported by its frequent allelic deletion during this transformation[16] One of the most frequent genetic abnormalities that occur in advanced colorectal cancer is loss of heterozygosity (LOH) of DCC in region 18q21. DCC elimination is not believed to be a key genetic change in tumour formation, but one of many alterations that can promote existing tumour growth.

K-RAS

Kirstein rat sarcoma (K-RAS) is a member of the RAS family of genes and present one of the most prominent proto-oncogenes in colon carcinogenesis. The RAS family genes encode highly conserved proteins that are involved in signal transduction. One major function of the RAS protein family is to couple growth factors to the Raf-mitogen-activated protein (MAP) kinase-MAP signal transduction pathway, which leads to the nuclear expression of early response genes[22]. The K-ras gene encodes for a protein involved in signal transduction from the cell membrane to the nucleus[20]. Specific mutations of this gene result in constitutive activation of this signal pathway and increased colonocyte replication. These mutations are associated with exophytic growth of adenomas in the transition to carcinoma[21].

K-RAS mutations have been found in 37% - 41% of colon carcinomas and appear to occur relatively early in colorectal cancer formation[23][24]. The K-RAS mutations appear to follow APC mutations and are associated with advanced adenomatous lesions. Evidence for this model comes from the observation that small adenomas with APC mutations carry K-RAS mutations in approximately 20% of the tumours, whereas approximately 50% of more advanced adenomas have K-RAS mutations Thus, alterations of K-RAS appear to promote colorectal ancer formation early in the adenoma-carcinoma sequence by mediating adenoma growth[25][26].

Table 1: Molecular genetics of sporadic colorectal cancer

Gene	Chromosome location	Normal physiologic function of encoded protein	Clinical manifestations of mutation
APC	5q	Regulates cell growth and apoptosis	Homozygous somatic mutation associated with colonic adenomas.
K-RAS family	12q	Encodes a small GTP binding protein on cell membrane involved in transduction of mitogenic signals across cell membrane	Mutated in about one half of colon cancers; may act in an intermediate stage of carcinogenesis; mutation common in hyperplastic polyps.
p53	17q	Regulates G1 cell cycle and apoptosis	Critical in transition from late adenoma to early cancer.
DCC	18q	Encodes a neural cell adhesion molecule, facilitates apoptosis, tumor suppressor	Believed to promote progression to frank carcinoma.
Mismatch repair genes	Located on several chromosomes	Recognize errors in nucleotide matching of complementary chromosome strand and initiate excision of erroneous strand	Progressive accumulation of mutations throughout the genome in affected cells leading to hyper mutability and genetic chaos; mutations of oncogenes or tumor suppressor genes can lead to colon cancer

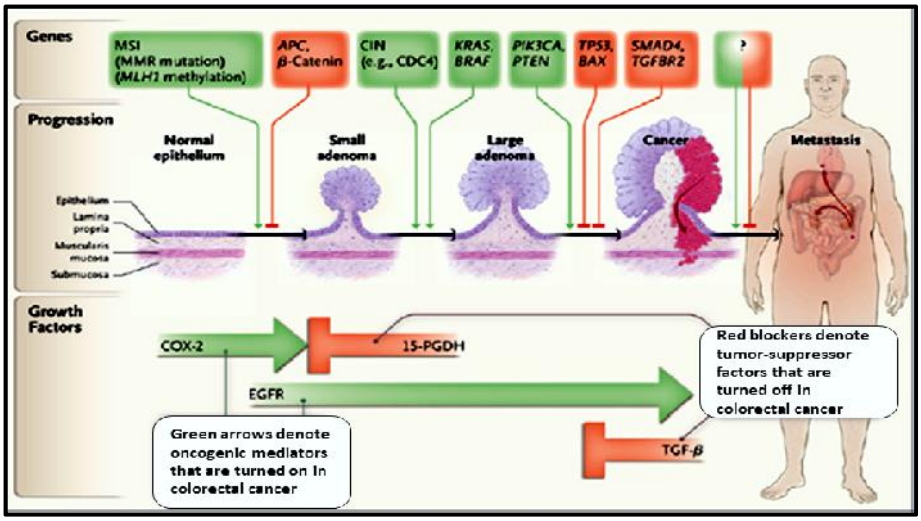

Figure 1: Genes and Growth Factor Pathways That Drive the Progression of Colorectal Cancer.

B. Epigenetic Alterations

Epigenetic silencing of genes, mostly mediated by aberrant DNA methylation, is another mechanism of gene inactivation in patients with colorectal cancer[27][28]. The term DNA methylation refers to the methylation of cytosine residues (5-methyl cytosine) at CpG sites found throughout the genome[29]. These epigenetic alterations are characteristically clustered in called CpG islands in gene promoter regions, and hypo and hyper methylation of these regions are related to activation and inhibition of transcription, respectively. This type of gene regulation is essential to cell differentiation as well as embryological development [30]. This aberrant promoter associated methylation can induce epigenetic silencing of gene expression[27]. In sporadic colorectal cancer with microsatellite instability, somatic epigenetic silencing blocks the expression of MLH1[27].

Genetic classification of CRC

Colorectal cancer is classified in to three forms: Sporadic (60%) comprises patients with no notable family history and, by definition, with no identifiable inherited gene mutation that accelerates cancer development**,** Familial (30%) refers to patients who have at least one blood relative with CRC or an adenoma, but with no specific germline mutation or clear pattern of inheritance**,** and hereditary syndromes (10%) which result from germline inheritance of mutations in highly penetrant cancer susceptibility genes[31].

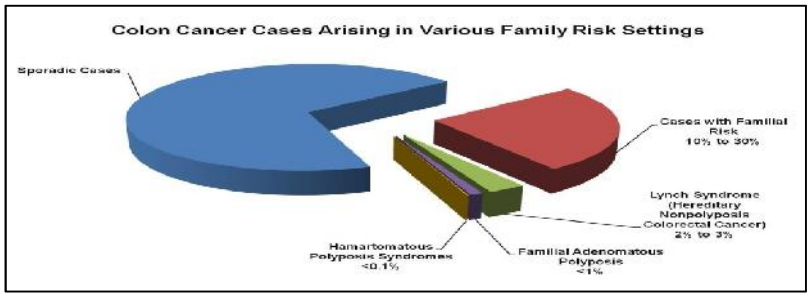

Figure 2: Types of colorectal cancer cases that arise in various family risk setting

Genetic instability of CRC

The loss of genomic stability can drive the development of colorectal cancer by facilitating the acquisition of multiple tumor-associated mutations. In this disease, genomic instability takes several forms, each with a different cause table 2[32]. The most common is termed the chromosomal instability pathway and accounts for 70% to 85% of colorectal cancers . These tumours are characterized by mutations in APC, P53, and KRAS and by frequent allelic loss at 18q[33] The microsatellite instability (MSI) pathway, comprising the remaining 15% of colorectal cancers, is characterized by loss of proficiency of the DNA mismatch repair (MMR) system and MSI.

Table 2: Patterns of Genomic Instability in CRC

Type of Instability and Syndrome	Type of Defect	Genes Involved	Phenotype
Chromosomal instability - loss of heterozygosity at multiple loci	Somatic	Loss of heterozygosity at APC,TP53, SMAD4	Characteristic of 70 to 85% of sporadic CRCs, depending on Stage.
DNA mismatch-repair defects Hereditary nonpolyposis colon cancer	Germ-line	MLH1, MSH2, MSH6 germ-line gene mutations	Multiple primary CRCs, accelera- ted tumor progression, and increased risk of endometrial, gastric, and urothelial tumors.
Sporadic colorectal cancer with mismatch-repair deficiency	Somatic	MLH1somatic methylation	CRC with increased risk of poor differentia- tion, more com- monly located in right colon, less aggressive clinical behavior than tumors without mismatch -repair deficiency.
MSI-CpG island methylator phenotype — methylation target loci	Somatic	Target, loci MLH1, MINT1,MINT2, MINT3	Characteristic of 15% of CRC, with most showing mismatchrepair deficiency from loss of tumor MLH1. expression
Base excision repair defect—MYH- sociated polyposis	Germ-line	MYH (denotesmutY homologue.)	Development of 15 or more colorectal adenomas with increased risk of colorectal cancer.

SUMMARY

Colorectal cancer is probably caused by a complex interaction between many genetic and environmental factors over time. More and large studies with informations on life style factors are required to assess these very possible gene-environment interactions. Studies that aid in the understanding of colorectal cancer on a molecular level have provided important tools for genetic testing for high-risk familial forms of the disease, predictive markers for selecting patients for certain classes of drug therapies, and molecular diagnostics for the noninvasive detection of early cancers.

REFERENCES

[1] F. Arvelo, F. Sojo, and C. Cotte, "Biology of colorectal cancer," Ecancermedical science, vol. 9, 2015, pp. 520-526.

[2] G.T. Deans, C.C. Patterson, T.G Parks, and et al. "Colorectal carcinoma: importance of clinical and pathological factors in survival". Ann R Coll Surg Engl, vol. 76, 1994; pp. 59–64.

[3] T. Kanazawa, T. Watanabe, S. Kazama, T. Tada, S. Koketsu, and H. Nagawa, "Poorly differentiated adenocarcinoma and mucinous carcinoma of the colon and rectum show higher rates of loss of heterozygosity and loss of E-cadherin expression due to methylation of promoter region," Int J Cancer, vol. 102,2002, pp. 225-229.

[4] H.S. Cooper, J.R. Slemmer. "Surgical pathology of carcinoma of the colon and rectum". Semin Oncol vol. 18, 1991; pp. 367–380.

[5] I.S. Sandhu, M.S. Bhutani. "Gastrointestinal endoscopic ultrasonography". Med Clin North Am vol.86, 2002, pp1289–1317.

[6] E.R. Fisher, R. Sass, A. Palekar A, and et al. "Dukes' classification revisited: findings from the national surgical adjuvant breast and bowel projects (protocol R-01) ". Cancer, vol 64, 1989, pp 2354– 2360.

[7] E.R. Fearon, R eric . and B. Vogelstein. "A genetic model for colorectal tumorigenesis". Cell,vol 61,1990, pp 759-767.

[8] C. Lengauer, K.W. Kinzler, and B. Vogelstein. "Genetic instabilities in human cancers". Nature, vol 396, 1998 , pp 643- 649.

[9] B. Vogelstein, and K.W. Kinzler. "Lessons from hereditary colorectal cancer". Cell, vol **87**, 1996, pp 159-170.

[10] N. Suraweera, A. Duval, M. Reperant, and et al. " Evaluation of tumor microsatellite instability using five quasimonomorphic repeats and pentaplex PCR". Gastroenterology vol 123, 2002; pp1804–1811.

[11] K.W. Kinzler, B. Vogelstein. " The genetic basis of human cancer".. In: B.Vogelstein, K.W. Kinzler. 2nd ed. New York: McGraw-Hill, 2002, pp 583-612.

[12] E.R. Fearon, G.T. Bommer . Molecular biology of colorectal cancer. In: T. Vincent, J.R. Devita, T.S. Lawrence, S.A. Rosenberg, eds. DeVita, Hellman, and Rosenberg's cancer: " principles & practice of oncology". Vol. 1. Philadelphia: Lippincott Williams & Wilkins, 2008, pp 1218-1231.

[13] K.H. Goss, J.Groden. " Biology of the adenomatous polyposis coli tumor suppressor". J Clin Oncol, vol. 18 , 2000, pp 1967-1979.

[14] D.H. Robbins, S.H. Itzkowitz. "The molecular and genetic basis of colon cancer". Med Clin North Am, vol. 86, 2002, pp 1467–1495.

[15] S.J. Baker, E.R. Fearon, J.M. Nigro, Hamilton SR, and et al. "Chromosome 17 deletions and p53 gene mutations in colorectal carcinomas". Science vol. 244, 1989, pp 217–221.

[16] B. Vogelstein, E.R. Fearon, S.R. Hamilton, and et al. "Genetic alterations during colorectal-tumor development". New England Journal of Medicine, vol **319**,1988, pp 525-532.

[17] M. Ohue, N. Tomita, T. Monden, and et al. "A frequent alteration of P53 gene in carcinoma in adenoma of colon". Cancer Research, **vol 54**,1994, pp 4798-4804.

[18] R. Kikuchiyanoshita, M. Konishi, S. Ito, and et al. "Genetic changes of both P53 alleles associated with the conversion from colorectal adenoma to early carcinoma in familial adenomatous polyposis and nonfamilial adenomatous polyposis patients". Cancer Research, **vol 52**,1992, pp 3965- 3971.

[19] D.P. Lane,. "Cancer—A death in the life of P53". Nature, vol **362**,1993, pp 786-787.

[20] R.J Slebos, S. Rodenhuis. "The ras gene family in human non-small-cell lung cancer". J Natl Cancer Inst Monogr vol 13, 1992, pp 23–29.

[21] M. Yashiro, J.M Carethers, L Laghi, Saito K, and et al. " Genetic pathways in the evolution of morphologically distinct colorectal neoplasms". Cancer Res, vol 61, 2001; pp 2676–2683.

[22] G.M. Bokoch, and C.J. Der. "Emerging concepts in the ras superfamily of Gtp-binding proteins". FASEB Jour- nal, vol **7**, 1993, pp 750-759.

[23] N. Arber, I. Shapira, J. Ratan, and et al. "Activation of K-ras mutations in human gastrointestinal tumors". Gastroenterology,vol **118**,2000, pp 1045-1050.

[24] J.L Bos, E.R. Fearon, S.R. Hamilton, and et al. "Prevalence of ras gene-mutations in human colorectal cancers". Nature, **vol 327**, 1987, pp 293-297.

[25] **S.M.** Powell, N. Zilz, Y. Beazer-Barclay, and et al. "APC mutations occur early during colorectal tumorigenesis". Nature, vol 359, 1992, pp 235-237.

[26] J. Tsao, and D. Shibata. "Further evidence that one of the earliest alterations in colorectal carcinogenesis involves APC". American Journal of Pathology, **vol 145**,1994, pp 531- 534.

[27] J.P. Issa. "CpG island methylator phenotype in cancer". Nat Rev Cancer vol 4,2004; pp 988-993.

[28] Y. Kondo, J.P. Issa. " Epigenetic changes in colorectal cancer". Cancer Metastasis Rev vol 23, 2004, pp 29-39.

[29] B.H. Ramsahoye, C.S. Davies, and K.I. Mills. "DNA methylation: Biology and significance". Blood Reviews, **vol 10**,1996, pp 249-261.

[30] M. Monk. "Epigenetic programming of differential gene-expression in development and evolution". Devel- opmental Genetics, vol 17,1995, pp 188-197.

[31] J.L. Ivanovich, T.E. Read, D.J. Ciske, and et al. "A practical approach to familial and hereditary colorectal cancer". American Journal of Medicine, **vol 107**,1999, pp 68-77.

[32] C. Lengauer, K.W. Kinzler, B. Vogelstein. "Genetic instability in colorectal cancers". Nature, vol 386, 1997, pp 623-627.

[33] S. Popat and R,S. Houlston. "A systematic review and meta-analysis of the relationship between chromosome 18q genotype, DCC status and colorectal cancer prognosis". European Journal of Cancer, **vol 41**,2005, pp 2060-2070.

Seroprevalence of *Toxoplasma gondii* among pregnant women in Misurata, Libya

Salem Ramadan Sariti[1], Mohamed Ali Al-Gazal[2] and Randa Mohamed Elsalhi.[2]

[1]-Libyan Academy-Misurata. [2]-Faculty of Medical Technology-Misurata

Abstract— *Toxoplasma gondii* infections in humans can only be detected by antibody levels and the current analysis is based on the prevalence of *T. gondii* specific IgG and specific IgM. This study aimed to determine the prevalence of pre-pregnant *T. gondii* infection among the women during the first trimester prior of pregnancy (old infection) in Misurata City and to determine the prevalence of *T. gondii* infection among the women during the first trimester prior of pregnancy (new infection) in Misurata City. A total of 300 blood samples were collected from pregnant women during the first trimester prior of pregnancy, residing in different localities of Misurata city. All samples were examined by Latex Agglutination Test and Elecsys-Cobas e analyzer test for Toxo IgG and IgM. The results highlights a total of 80 positive samples (26.7%) have been detected by the Latex Agglutination Test, this result was similar to the Elecsys-Cobas e analyzer test for Toxo IgG. In contrast, Just three samples were positive by Elecsys-Cobas e analyzer test for Toxo IgM (1%). In addition to one positive sample detected by Elecsys-Cobas e analyzer test for both Toxo IgG and Toxo IgM in the same time. There was no significant difference ($p>0.05$) between Latex Agglutination Test and Elecsys-Cobas e analyzer test for Toxo IgG. Whereas, a clear significant difference ($P = 0.0105$) between Latex Agglutination Test and Elecsys-Cobas e analyzer test for Toxo IgG on one side versus Elecsys-Cobas e analyzer test for Toxo IgM on the other side. As for the overall prevalence, our results showed 82 infected sample for *T. gondii* (27.3%). The risk and severity of congenital toxoplasmosis are greatest when acquired during the first three months of pregnancy. Due to the above results there are no dangers of the disease. serological follow-up during pregnancy are of great importance in the prevention of congenital toxoplasmosis.

Keywords- Prevalence, *Toxoplasma gondii* and Latex Agglutination Test.

INTRODUCTION

Toxoplasma gondii, a protozoan parasite which responsible for a range of human and animal diseases and have considerable medical and economic impact worldwide [(4)]. Like the other members of the phylum Apicomplexa, T. gondii, is characterized by a specialized apical end which conceited with the process of host invasion [(13)]. Moreover, it is also an obligate intracellular parasite, growing and replicating only within host cells. Parasite replication occurs after invasion of a host cell, within a membrane-bound parasitophorous vacuole, and continues until the host cell is lysed by the replicating parasites [(14)].

1-Epidemiology:

T. gondii is a ubiquitous protozoan parasite, chronically infecting 10–90% of human populations worldwide. Sexual differentiation occurs only in the cat, but asexual *T. gondii* parasites can invade, proliferate, and encyst in virtually any nucleated cell. Primary infection during pregnancy poses a risk of abortion or severe birth defects or miscarriage of the fetus [(5)].

Human infections with T.gondii may be acquired from food or soil contamination and water contamination. Due to the potential threat to public health from intentional dispersal into the population, T.gondii and Cryptosporidium parvum are listed as 45 Category B Biodefense Pathogens by the National Institutes of Health [3].

In Tripoli-Libya, Gashout et al. (2008) have determined 17.6% as acute or recent infections and 45% as immunized or old infections of toxoplasmosis among 692 women who suffered spontaneous abortion and attended the Department of Obstetrics and Gynecology of the Tripoli Central Hospital [6].

2.Pathogenesity during pregnancy:

Congenital toxoplasmosis only occurs when the mother has an active infection during pregnancy. The risk and severity of congenital toxoplasmosis are greatest when acquired during the first three months of pregnancy [2&9]; but in general, there is no increased risk to the fetus when toxoplasmosis occurs more than 6 months prior to conception [15]. Moreover, toxoplasmosis can develop into a severe systemic illness when it is in congenital form, in which the mother, when infected for the first time during pregnancy, can present a temporary parasitemia with focal lesions generated within the placenta, thereby infecting the fetus [11]. The parasite reaches the fetus transplacentally, causing various degrees of damage, depending on the virulence of the parasite, on the immune response of the mother and on the pregnancy period of the woman when infected, resulting in fetal death or in severe clinical symptoms [16]. It can also develop during the birth of normal children that later present's retinochoroiditis alteration, provoking mental and psychomotor disorders [11]. However, primary infection acquired during

pregnancy may result in severe damage to the foetus [10&12]. Manifestations of congenital toxoplasmosis include mental retardation, seizures, blindness, and death [8].

3.Serological testing for toxoplasmosis:

T. gondii infections in humans can only be detected by antibody levels and the current analysis is based on the prevalence of *T. gondii* specific IgG (evidence of earlier (or old) infection, peaking at 4 months after infection and persisting at low levels for life) and on *T. gondii* specific IgM (evidence of current (or new) infection, appearing within 1–2 weeks of infection and subsiding by 6–9 months) [1&17].

4.Statement of purpose:

Awareness of the dangers of the disease and serological follow-up during pregnancy are of great importance in the prevention of congenital toxoplasmosis [7]. In addition, understanding and screening the infectious rate and the risk of this parasite in Misurata City, is therefore essential for the development of improved treatment and further biological and medical studies.

5.Study objectives:

This study aimed to determine the prevalence of pre-pregnant *T. gondii* infection among the women during the first trimester prior of pregnancy (old infection) in Misurata City and to

determine the prevalence of *T. gondii* infection among the women during the first trimester prior of pregnancy (new infection) in Misurata City.

MATERIALS AND METHODS:

A total of 300 blood samples were collected from pregnant women during the first trimester prior of pregnancy, residing in different localities of Misurata city.

All samples were examined by Latex Agglutination Test and Elecsys-Cobas e analyzer for Toxo IgG and IgM Test.

1.Latex Agglutination Test; which have been serologically examined to detect both IgG and IgM in the same time (non-specific test).

Interpretation of result:

-Negative for Toxo-Ab: No agglutination (homogenous appearance).

-Positive for Toxo-Ab: Distinct agglutination indicates a content of Toxo-Ab.

2.Elecsys-Cobas e analyzer test for Toxo IgG and IgM; which have been serologically examined for the presence of toxoplasma-specific IgG and toxoplasma-specific IgM antibodies separately (each independent on the other).

3.Statistical analysis was performed by the One Way ANOVA, using chi square test. A probability (p) value of less than and/or equal to 0.05 was considered as significant whenever appropriate.

RESULTS

A total of 300 blood samples were serologically examined for the presence of toxoplasma-IgG and IgM. The results highlights a total of 80 positive samples (26.7%) have been detected by the Latex Agglutination test, this result was similar to the Elecsys-Cobas e analyzer test for Toxo IgG, which represented the old infection (Table 1).

Table 1: The positive samples obtained by the two usemethods.

Samples Examined	Number and percentage of positive samples by different methods		
	Latex Agglutination Test	Elecsys-Cobas e analyzer	
300	For both IgG and IgM	For toxoplasma-specific IgG	For toxoplasma-specific IgM
	80 (26.7%)	80 (26.7%)	3 (1%)

Figures in parentheses indicate percentages.

In contrast, just three samples were positive by Elecsys-Cobas e analyzer test for Toxo IgM (1%), which represented the new infection. Our results showed one sample that was positive by Elecsys-Cobas e analyzer test for both Toxo IgG test and Toxo IgM test (0.33%). In another meaning, the overall prevalence was 82 infected sample (27.3%).

There was no significant difference (p>0.05) between Latex Agglutination test and Elecsys-Cobas analyzer test for Toxo IgG. Whereas, a clear significant difference (P=0.0105) between Latex Agglutination test versus Elecsys-Cobas e analyzer test for Toxo IgM. In the same way, there was a clear significant difference (P=0.0105) between Elecsys-Cobas e analyzer test for Toxo IgG versus Elecsys-Cobas e analyzer test for Toxo IgM.

As for the previous abortion, the results showed 64 sample (21.3%) of the total examined samples were positive and had have no previous abortion, whereas 9 samples (3%) had one time abortion and 9 samples (3%) had two times abortion (Table 2).

For the abortion frequency, the results illustrated no significant difference (p>0.05) when compared to the number of those having no abortion.

Table 2: Number of the positive samples in correlation with previous abortion

Samples Examined	The abortion frequency No. of positive samples (percentage)		
300	Non	One time	Two times
	64 (21.3%)	9 (3%)	9 (3%)

DISCUSSION

The worldwide prevalence of *T. gondii* ranged between 10 to 90% of human populations [(5)]. Within this range, the current results showed a prevalence of 27.3%.

We determined 0.6% as acute or recent infections and 26.7% as immunized or old infections of toxoplasmosis compared to 17.6% as acute or recent infections and 45% as immunized or old infections of toxoplasmosis obtained by Gashout et al. (2008) in Tripoli-Libya [(6)].

Toxoplasmosis can be acquired from several sources such as handling cats and food, soil and water contamination [(3)]. Due to the above infection ranges, we could say that there is a good hygiene and in the same line, the people have a good health education.

Primary infection during pregnancy poses a risk of abortion or severe birth defects or miscarriage of the fetus [(5)]. Due to the above results, there are no abortion dangers of the infection with T. gondii. serological follow-up during pregnancy are of great importance in the prevention of congenital toxoplasmosis.

Our results illustrated that latex agglutination test might be used to determine the general sero-prevalence of the *T. gondii* parasite, whereas to determine the new and the old infections separately, a specific *T. gondii* IgG test and a specific *T. gondii* IgM test should be used (such as Elecsys-Cobas e analyzer test or ELISA).

CONCLUSION:

The risk and severity of congenital toxoplasmosis are greatest when acquired during the first three months of pregnancy. Due to the above results, there are no abortion dangers of the disease. serological follow-up during pregnancy are of great importance in the prevention of congenital toxoplasmosis.

CONCLUSION

Hot particle hazards exist in the nuclear power industry, in the processing of radioactive ore, in medical, industrial and research applications of radioactive isotopes and around accelerators. The current work is an extension to a previous work for evaluating Monte Carlo code and different measurement techniques in measuring spatial dose distributions around high energy emitting ^{106}Ru/Rh model hot particle. For radiological protection purpose, the agreement between measurements and calculations is good. An overall revision of this work with that of ^{60}Co and ^{170}Tm is required. Furthermore, the effect of geometrical shape of hot particles directly put on the skin should be investigated to reflect the real situation of hot particles in the environment.

REFERENCES

[1] **-Abu-Madi** Marawan A, Naema Al-Molawi and Jerzy M Behnke. (2008) Seroprevalence and epidemiological correlates of *Toxoplasma gondii* infections among patients referred for hospital-based serological testing in Doha, Qatar. Parasites & Vectors. 1:39

[2] **-Adesiyun** AA, Gooding R, Ganta K, Seepersadsingh N, Rainsewak S.(2007) Congenital toxoplasmosis in two health institutions in Trinidad. West Indian Med J . 56:166-170.

[3] **-Aurrecoechea** Cristina, Heiges Mark, Wang Haiming, Wang Zhiming, Fischer Steve, Rhodes Philippa, Miller John, Kraemer Eileen, Stoeckert Christian J., Roos David S., and Kissinger Jessica C. ApiDB (2006) integrated resources for the apicomplexan. Nucleic Acids Research. Vol. 00, Database issue D1–D4 doi:10.1093/nar/gkl880 bioinformatics resource center.

[4] **-Black,** M. W. and Boothroyd, J. C.(2000) Lytic cycle of *Toxoplasma gondii*. Microbiol. Mol. Biol. Rev. 64, 607-623.

[5] **-Dubey,** J.P.(1998) Advances in the life cycle of *Toxoplasma gondii*. Int. J. Parasitol. 28, 1019–1024.

[6] **-Gashout** Aisha , Taher Lazrag, Huda Gashut, Tawfig Swedan: Qualitative assessment of risk for spontaneous abortion associated with toxoplasma and rubella (2008) immunity appraisal. The Libyan Journal of Infectious Diseases Vol. 2 No. 1, 52:56.

[7] **-Hill** D., Dubey J.P.(2002) *Toxoplasma gondii*: transmission, diagnosis and prevention. Clin Microbiol Infect 8:634-40.

[8] **-Jones** JL, Lopez A, Wilson M, Schulkin J, Gibbs R: Congenital toxoplasmosis (2001) a review. Obstet Gynecol Surv 56:296-305.

[9] **-Jumaian** NF.(2005) Seroprevalence and risk factor of toxoplasma infection in pregnant women in Jordan. East Mediterr Health 11:45-51.

[10] **-Kravetz** JD, Federman DG. (2005) Toxoplasmosis in pregnancy. Am J Med 118:212-216.

[11] **-Lopes** Fabiana Maria Ruiz, Gonçalves Daniela Dib, Mitsuka-Breganó Regina, Freire Roberta Lemos and Navarro Italmar Teodorico (2007)*Toxoplasma gondii* Infection in Pregnancy. The Brazilian Journal of Infectious Diseases 11(5):496-506.

[12] **-Montoya** JG, Liesenfeld O. (2004) Toxoplasmosis. Lancet 363:1965-1976.

[13] **-Morrissette** Naomi S., Bedian Vahe, Webster Paul, and Roos David S.(1994) Charactrization of Extreme Apical Antigens from *Toxoplasma gondii*. Experimental Parasitology 79, 445-459.

[14] **-Morrissette** Naomi S. and Sibley L. David (2001) Disruption of microtubules uncouples budding and nuclear division in *Toxoplasma gondii*. Journal of Cell Science 115, 1017-1025.

[15] **-Organization** of Teratology Information Specialists [OTIS] (2007)Toxoplasmosis and Pregnancy, January.

[16] **-Spalding** S.M., Amendoeira M.R.R., Ribeiro L.C., et al.(2003) Estudo prospectivo de gestantes e seus bebês com risco de transmissão de toxoplasmose congênita em município do Rio Grande do Sul. Rev Soc Bras Med Trop 36:483-91.

[17] **-Sukthana** Y. (2006) Toxoplasmosis: beyond animals to humans. Trends in Parasitol 22:137-142.

The Second Symposium on Theories and Applications of Basic and Biosciences Vol. (2) Issue (1)

Laser-plasma wakefield acceleration in tapered capillary discharge waveguides

Salima S. Abuazoum
Email: saliazoum@gmail.com

Abstract— Enhancing the electron bunch properties in a laser wakefield accelerator by tapering the longitudinal plasma density has been experimentally demonstrated. Comparison has been made between density (i) increasing with distance (positive taper), (ii) constant (no taper) and (iii) decreasing with distance (negative taper). All three produce narrow energy spread, low divergence electron bunches but a mean enhancement of 22% (from 205 MeV to 250 MeV) for the central energy is obtained with a positive taper. A negative taper exhibits improved pointing angle (0.4 mrad) and stability (1.7 mrad r.m.s.).

Keywords- Hot Particles, Radiation Dosimetry, EGSnrc, Monte Carlo, Imaging Photon Detector, Extrapolation Chamber, RadioChromic Dye Film, Non-uniform Dose Distribution, Skin Dosimetry. Radiological Protection.

INTRODUCTION

The basis of the laser-plasma wakefield accelerator (LWFA) is the creation of a very large accelerating gradient (~1 GeV/cm) by a terawatt- or petawatt-scale laser pulse focused into underdense plasma and a wide variety of recent experiments have illustrated its potential for serving as ultra-compact next-generation sources of high energy particle and radiation beams [1,2]. Benchmark demonstrations include the first monoenergetic electron beams [3,4,5] generated in the 100-200 MeV range, 1 GeV monoenergetic electron beams [6] produced with a 40 TW laser, LWFA- driven undulator synchrotron radiation in the visible [7] and soft X-ray [8] spectral regions and LWFA-driven gamma-ray betatron radiation [9]. Two of these experiments [6,9] utilised as the accelerating medium a gas-filled capillary discharge waveguide (CDW) which supports operation at lower plasma density (n ~10^{18} cm^{-3}), as compared with gas jets [3,4,5,7,11], thus leading to higher electron energies (n^{-1}) [10]. Lower plasma densities are also supported in gas cells [8,12], that can simply be a CDW without the discharge, and plastic ablative CDWs [13,14], that are not as robust as sapphire or alumina gas-filled CDWs.

Future LWFA-based light source and collider user facilities will have less stringent laser requirements if the electron energy can be increased for a given laser power, for example, generating GeV energies suitable for driving an X- ray free-electron laser with a more compact, almost turn-key10 TW laser system. Energy gain in a homogeneous plasma is limited by dephasing (electrons out-running the accelerating phase of the wake and eventually losing energy) and the idea of introducing a longitudinal plasma density gradient (tapering) to offset dephasing has been around since the 1980s [15]. Theoretical studies have predicted significant energy increase [16,17] and, in this letter, we report on the first experimental confirmation of energy enhancement in a LWFA protection applications the International Commission on Radiological Protection ICRP recommends the use of a depth of 70 µm and the dose is averaged over an area of 1cm^2 [9-10] with a tapered plasma density (increasing with

distance Implementing the taper has been achieved in gas-filled CDWs by applying a femtosecond laser micromachining production technique [18] and efficient laser pulse guiding has been confirmed at low intensity [19]. Previous ablative CDWs with a linear taper have been produced [20] but no acceleration studies have been reported. In addition to energy enhancement, significant reduction of beam pointing angle and stability is obtained for oppositely tapered density (decreasing with distance).

A Ti:sapphire laser pulse (energy = 800 mJ, full-width at half-maximum duration = 40 fs and wavelength $_0$ = 800 nm) is focused to a (radius at $1/e^2$) waist w_{0L} = 20 m at the entrance plane of the capillary under investigation such that, initially, the power = 20 TW, intensity = 1.6 10^{18} W/cm^2 and normalized vector potential a_0 = eE/m_0c $_0$ = 0.9 where E is the electric field strength, c is the speed of light in vacuum, $_0$ = 2 c/ $_0$ and e and m_0 are the electron charge and rest mass respectively. Before the laser pulse enters the capillary, hydrogen gas is injected at a backing pressure of 140-200 mbar and an underdense plasma is formed by applying a22 kV, 900 ns voltage pulse between two electrodes located at either end of the capillary [22].Measurement of a transient current pulse, peaking at ~300 A (in our case), is evidence of a high degree of ionization [23]. Thermal conduction to the capillary walls sets up a parabolic radial profile in the electron density distribution and laser diffraction can be exactly compensated by plasma lensing enabling efficient transport over several centimetres with little energy loss and excellent mode structure [24]. However, relativistic self-focussing and photon acceleration can still occur, thus helping to produce a trailing evacuated bubble into which electrons are injected from the background plasma.

Table 1 summarizes the properties of the pertinent CDWs that are labeled TP, S and TN respectively. In each capillary, an estimate of the on-axis density has been obtained with Raman spectroscopy of the transmitted laser pulse [25], as shown in Fig. 1(a) for capillary TP. In the case of tapered channels, this diagnostic provides the average (or midpoint) density, with the estimated start-to-end density change determined by the corresponding cross-section change [19]. The density values are consistent with Raman [25], interferometer [26,27], Stark-broadened spectroscopy [19,27] and betatron radiation [9] measurements obtained in similar CDW experiments.

Table 1. Diameter D, taper rate = D/2L, where D is the diameter change over length L (= 40 mm in each case), and measured on-axis plasma density n for each capillary type. The density tapers for types TP and TN are estimated from the respective taper rates.

Name	TP	S	TN
Taper	Positive	Zero	Negative
D (m)	282 230	230	206 268
(10^{-4})	6.25	0	8.0
n (10^{18} cm^{-}	3.1 (2.5 3.8)	3.5 - 5.7	3.6 (4.7 2.8)

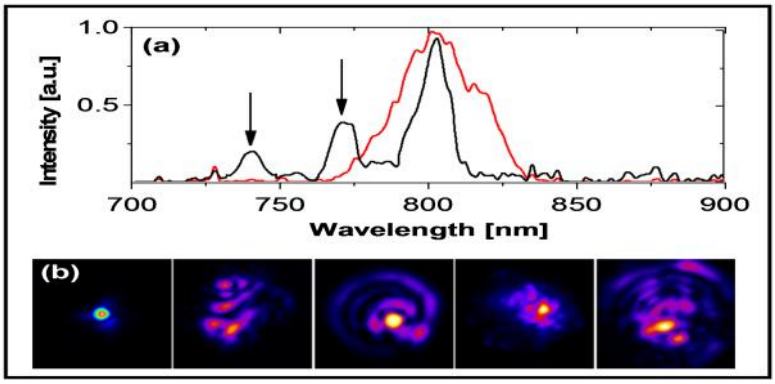

Fig. 1 (color online). (a) Laser spectrum before (red) and after (black) propagation and electron beam generation in capillary TP. Arrows indicate anti-Stokes peaks. (b) Example images from left to right of: laser focal spot, poor guiding in TN and good guiding in TP, S and TN respectively

Guiding of high-power laser pulses in each capillary is comparable in terms of transmitted laser energy and mode structure. For our laser conditions, the entrance laser beam waist is less than the matched waist, w_{0M} [m] 1.48 10^5 $R_{we}^{1/2}$[m] / $n^{1/4}$[cm^{-3}] where R_{we} is the entrance radius, that introduces a periodic oscillation in the transverse beam profile (scalloping) as it propagates along the waveguide [23]. In our case, w_{0M} 32-44 m compared to w_{0L} = 20 m. Despite being far from the matched condition, however, reasonable energy transmission of (67 10)% is obtained for all three capillary types at the laser-discharge synchronization timing for best guiding [Fig. 1(b)], confirming that guiding is equally efficient in the presence of a density taper [19]. In each case, later timing results in reduced transmission of (30 10)% due to plasma wake formation and subsequent electron beam production [25].

At relativistic intensities, after initial waveguiding, electron beam propagation in a CDW is dominated by self- focusing, i.e., the waveguide influences the propagation only at the beginning of the interaction. This is evident in our observations that virtually no electron beam production was achieved in a larger diameter (300 m) straight capillary, in agreement with other experiments in this laser intensity range [6, 24], nor in positively tapered capillaries with a similarly wide entrance diameter (320 270 m or 305 183 m). When the channel entrance is too wide, the initial beam diffraction is too great for subsequent self-focusing, strong wake generation and self-trapping of electrons. Furthermore, even the capillary type S with diameter 230 m struggled to self-inject at lower plasma densities, hence, the density was typically increased (Table 1) to facilitate injection in this capillary.

The beam profile of electron beams exiting each capillary have been captured on a Lanex screen located 0.6 m downstream and imaged by a charged-coupled device (CCD) camera. Table 2 summarizes the beam relative charge, divergence and pointing behavior collected in large data sets. The relative charge data collected on this uncalibrated screen, that also contain the low energy tail, are consistent with absolute charge measurements for the high energy bunches (see later). Most charge was injected into the bunch, on average, in the capillary TP. Perhaps the positive density gradient favors greater laser self-focusing.

Table 2. Beam profile data giving the mean (minimum) electron beam relative charges Q_{rel}, r.m.s. divergences θ and pointing angles φ in the vertical Y and horizontal X planes respectively for each capillary type where each uncertainty is the r.m.s. standard deviation.

Name	TP	S	TN
Number of shots	88	68	100
Mean Q_{rel} [a.u.]	2.6 ± 4.8	0.5 ± 0.4	1.5 ± 2.1
Mean (Min.) θ_Y [mrad]	3.3 ± 2.0 (0.8)	1.6 ± 0.9 (0.7)	2.1 ± 1.7 (0.6)
Mean (Min.) θ_X [mrad]	3.5 ± 2.5 (0.9)	1.8 ± 1.2 (0.7)	1.5 ± 1.1 (0.5)
Mean φ_Y [mrad]	-2.3 ± 6.6	-19 ± 10	-0.4 ± 2.1
Mean φ_X [mrad]	2.0 ± 7.6	9.0 ± 13	0.3 ± 1.3

As shown in Fig. 2(a), the mean beam r.m.s. divergence for each is in the range 1.3-3.3 mrad with the best shots less than 1 mrad, down to just 0.5-0.6 mrad for capillary TN. The divergence scales proportionately with the charge [21] which accounts for the larger divergence for capillary TP while the similar mean divergences for lower charge S and TN data indicate a lower intrinsic limit for the divergence and, thus, the transverse emittance, has been reached. Assuming a source size of 2-3 μm, the minimum normalized transverse emittance is estimated to be ~0.5 π mm mrad, consistent with pepper-pot emittance measurements in a gas jet accelerator that showed detection resolution-limited values of 1.1 π mm mrad [21].

Figure 2(b) illustrates the large differences in pointing angle and stability between the capillary types. Capillary S suffered from both a large angle and poor stability which may be a product of this accelerator operating extremely close to the injection threshold (one third of shots producing no electrons, all other shots with little charge). The highest quality capillary in terms of close-to-axis pointing angle (0.3-0.4 mrad in both axes) and smallest pointing fluctuations (just 1.3 mrad in the horizontal axis) was type TN. This may be related to the negative longitudinal plasma density gradient driving an increase in the accelerating bubble size as the interaction evolves.

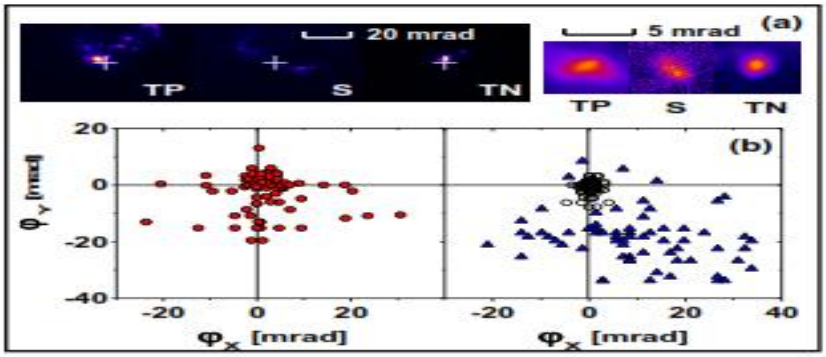

FIG. 2 (color online). (a) Example images of the beam profile and (b) pointing distribution for each capillary type (TP: red closed circle, S: blue triangle, TN: black open circle). The beam line axis is indicated by a white cross and the origin respectively.

Electron energy spectra have been obtained by transporting the electrons through a triplet of electromagnetic quadrupole magnets (each of field strength 120 mT) and an imaging magnetic dipole spectrometer (field strength B_{ES} = 0.91-1.25 T) [12]. A Ce:YAG crystal located at focal plane of the spectrometer is imaged with a CCD camera. The acceptance angle for the quadrupoles aperture is 8 mrad therefore the beam pointing (Table 2) impacts on the number of shots that are successfully captured in the electron spectrometer. The energy spectrum measurements are summarized in Table 3 for shots showing a discernable electron bunch of finite energy spread, with type TN (best pointing angle and Monoenergetic electron bunches with narrow energy spread are obtained in all three capillary types [Fig. 3(a)]

The bunches. In agreement with theory [15,16,17], positive tapering TP produces an energy enhancement (22% in the mean central energy of the electron bunch) with respect to capillary S. This behavior is reflected in the smaller converse energy reduction (−10% with respect to type S) obtained with negative tapering TN. Note that most of the type S data was acquired at the higher end of its applied density range ($\approx 5.7 \times 10^{18}$ cm^{-3}) where injection was relatively easier while in the density range directly comparable to the other capillary types ($\approx 3.5 \times 10^{18}$ cm^{-3}) no significant electron energy increase was observed. Comparing types TP and TN, the energy difference is apparent despite the respective densities being very closely matched.

The highest central energy for type TP was 290 MeV with upper electron energy of 320 MeV (Fig. 3(a)]. The energy enhancement obtained (20-40%) for a positive taper compares well with an analytical model [17] predicting ~100-300% gain for a linearly tapered accelerator when one compares the respective taper rates (0.33×10^{18} cm^{-3}/cm in our experiment, 3.5×10^{18} cm^{-3}/cm in the model). This is despite that model being solely for single particle acceleration, neglecting effects like laser pump depletion and self-focusing. Experimentally, therefore, type TP also represents a gentle taper rate and further optimisation of the micromachining manufacturing process [18] should increase the taper rate while still facilitating self-injection. Nevertheless, these results demonstrate

the success of applying a positive longitudinal plasma density gradient to boost the final electron energy.

Table 3. Energy spectrum data giving the mean (maximum) electron bunch charge Q, central energy E and measured absolute energy spread $\sigma_{\gamma MEAS}$ and the minimum measured relative energy spread $\sigma_{\gamma MEAS}/\gamma$ of the electron bunch for each capillary type where each uncertainty is the r.m.s. standard deviation.

Name	TP	S	TN
Number of shots	10	5	33
Mean (Max.) Q [pC]	2.6 ± 2.3 (6.6)	0.2 ± 0.1 (0.3)	1.3 ± 1.1 (5.1)
Mean (Max.) E [MeV]	250 ± 25 (290)	205 ± 5 (211)	184 ± 17 (229)
Mean (Min.) $\sigma_{\gamma MEAS}$ [MeV]	14 ± 8 (3.3)	4 ± 1 (2.0)	13 ± 5 (4.8)
Min. $\sigma_{\gamma MEAS}/\gamma$ [%]	1.6	1.0	2.6

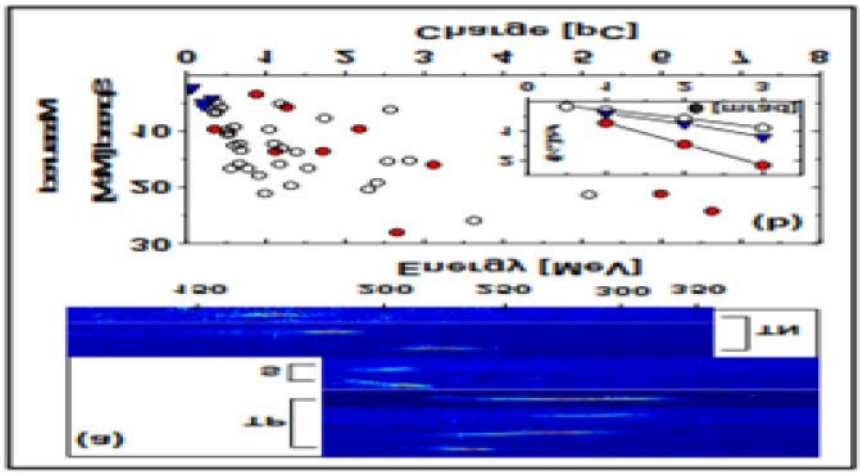

FIG. 3 (color online). (a) Example images of the energy spectrum and (b) absolute energy spread dependence on charge for each capillary type (TP: red closed circle, S: blue triangle, TN: black open circle). Electron spectrometer B_{ES} = 1.25 T except for type TN where B_{ES} = 0.91 T. Inset is the corresponding simulated r.m.s. spectrometer resolution R for each capillary calculated as a function of divergence θ at the respective mean central energy values

The dependence of the measured absolute energy spread on the charge is shown in Fig. 3(b) with all three capillary types conforming to the same overall dependence. Very low charge bunches arising from very low injection volumes lead to the smallest energy spreads [28] while, at higher charge, beam loading effects [29] may also act to broaden the energy spectrum.

The narrowest measured bunch r.m.s. relative energy spreads are in the range 1-2% (determined solely for that bunch and ignoring lower energy bunches or pedestals). Beam line simulations using the General Particle Tracer code [30] indicate that the electron spectrometer resolution is also in the 0.5-2.5% range for the typical bunch properties observed in experiment [inset of Fig. 3(b)]. Therefore, the narrowest spread bunches for types TP and S have been strongly convoluted by the detection system response and the true minimum energy spread is less than 1%, as has been observed for gas jet accelerators driven either by single [12] or colliding [28] laser pulses.

REFERENCES

1. V. Malka et al., Nature Phys. **4**, 447 (2008).
2. E. Esarey et al., Nature **431**, 535 (2004).
4. C. G. R. Geddes et al., Nature **431**, 538 (2004).
5. J. Faure et al., Nature **431**, 541 (2004).
6. W. P. Leemans et al., Nature Phys. **2**, 696 (2006).
7. H.-P. Schlenvoigt et al., Nature Phys. **4**, 130 (2008).
8. M. Fuchs et al., Nature Phys. **5**, 826 (2009).
9. S. Cipiccia et al., Nature Phys. **7**, 867 (2011).
10. W. Lu et al., Phys. Rev. ST Accel. Beams **10**, 061301 (2007).11. S. M. Wiggins et al., Plasma Phys. Control. Fusion **52**,
124032 (2010).
12. C. E. Clayton et al., Phys. Rev. Lett. **105**, 105003 (2010).
13. C. McGuffey et al., Phys. Plasmas **16**, 113105 (2009).
14. H. Lu et al., Appl. Phys. Lett. **99**, 091502 (2011).
15. T. Katsouleas, Phys. Rev. A **33**, 2056 (1986).
16. P. Sprangle et al., Phys. Plasmas **9**, 2364 (2002).
17. W. Rittershofer et al., Phys. Plasmas **17**, 063104 (2010).
18. S. M. Wiggins et al., Rev. Sci. Instrum. **82**, 096104 (2011).
19. S. Abuazoum et al., Appl. Phys. Lett. **100**, 014106 (2012).
20. D. Kaganovich et al., Appl. Phys. Lett. **75**, 772 (1999).
21. E. Brunetti et al., Phys. Rev. Lett. **105**, 215007 (2010).
22. S. Abuazoum et al., Rev. Sci. Instrum. **82**, 063505 (2011).
23. D. J. Spence and S. M. Hooker, Phys. Rev. E **63**, 015401 (2001).
24. T. P. Rowlands-Rees et al., Phys. Rev. Lett. **100**, 105005 (2008).
25. S. Karsch et al., New J. Phys. **9**, 415 (2007).
26. A. J. Gonsalves et al., Phys. Rev. Lett. **98**, 025002 (2007).
27. D. G. Jang et al., Appl. Phys. Lett. **99**, 141502 (2011).
28. C. Rechatin et al., Phys. Rev. Lett. **102**, 164801 (2009).
29. T. Katsouleas et al., Part. Accel. **22**, 81 (1987).
30. S. van der Geer et al., in Computational Accelerator Physics 2002 Vol. 175 (Institute of Physics, Bristol, UK, (2005), p 101.